EUROPEAN JOURNAL OF PURE AND APPLIED MATHEMATICS
2026, Vol. 19, Issue 2, Article Number 7019
ISSN 1307-5543 – ejpam.com
Published by New York Business Global

Quadri-Partition Neutrosophic Soft Topology and Dimensionality Reduction, Clustering, and Signal Recovery in High-Dimensional Spaces

Maha Mohammed Saeed[1], Dragan Pamucar[2**], Raed Hatamleh[3], Hamza Ali Abujabal[4], Arif Mehmood[5], Alaa M. Abd El-latif[6], Giorgio Nordo[7], Cris L. Armada[8,9]

[1] *Department of Mathematics, Faculty of Sciences, King Abdulaziz University, P.O. Box 80203, Jeddah 21589, Saudi Arabia*
[2] *Szechenyi Istvan University, Gyor, Hungary*
[3] *Department of Mathematics, Faculty of Science, Jadara University, P.O. Box 733, Irbid 21110, Jordan*
[4] *Department of mathematics, King Abdulaziz University, P.O. Box 80003, Jeddah 21589, Saudi Arabia*
[5] *Department of Mathematics, Institute of Numerical Sciences, Gomal University, Dera Ismail Khan 29050, KPK, Pakistan*
[6] *Department of Mathematics, College of Science, Northern Border University, Arar 91431, Saudi Arabia*
[7] *MIFT Department (Mathematical and Computer Science, Physical Sciences and Earth Sciences) - University of Messina, 98166 Sant'Agata, Messina, Italy.*
[8] *National University Ho Chi Minh City, Linh Trung Ward, Thu Duc City, Ho Chi Minh City, Vietnam*
[9] *Department of Applied Mathematics, Faculty of Applied Science, Ho Chi Minh City University of Technology (HCMUT), 268 Ly Thuong Kiet, Ward 14, District 10, Ho Chi Minh City, Vietnam*

Abstract. Quadri-partition neutrosophic soft locally compact spaces (QPNSLCS) of quadri-partition neutrosophic soft topological spaces (QPNSTS) are the concept introduced in this research. The theoretical foundation for the treatment of uncertainty in complex topological structures is strengthened by the fact that local compactness, particularly when combined with the Hausdorff condition, establishes the existence of compact neighborhoods and the compactness of subspaces. Parallel coordinate plots facilitate comparisons across multiple variables, PCA displays patterns of variance-based groupings, t-SNE in 2D and 3D displays patterns of similarity, and Figures 5.1 to 5.8 demonstrate various dimensionality reduction and clustering techniques to analyze high-dimensional data to support this theoretical discussion. The optimal number of clusters is estimated by the Elbow Method at K = 2, and comparisons between t-SNE and UMAP show that local and global structure preservations differ. Additionally, the purification of mixed signals with slight distortions is demonstrated using Independent Component Analysis (ICA). Together, these findings improve clustering mistakes, show structure patterns, reconstruct latent information, and offer a theoretical and practical knowledge of complicated data processing.

2020 Mathematics Subject Classifications: AMS Subject Classification: 54A05

Key Words and Phrases: Neutrosophic soft set, dNSSs, dNSTSs, local compactness, t-SNE, pCA, uMAP, iCA.

---

*Corresponding Author.
DOI: https://doi.org/10.29020/nybg.ejpam.v19i2.7019

Email addresses: `mmmohammed@kau.edu.sa` (M. M. Saeed), `pamucar.dragan@sze.hu` (D. Pamucar), `raed@jadara.edu.jo` (R. Hatamleh), `haabujabal@kau.edu.sa` (H. A. Abujabal), `mehdaniyal@gmail.com` (A. Mehmood), `alaa.ali@nbu.edu.sa` (A. M. Abd El-latif), `giorgio.nordo@unime.it` (G. Nordo), `cris.armada@hcmut.edu.vn` (C. L. Armada)

1. Introduction

Since Zadeh [1] developed fuzzy sets, which replaced classical binary membership with a continuous degree of membership, mathematical notions of uncertainty and imprecision have undergone a drastic transformation. It was made possible by this paradigm change to approach vagueness in a way that is more representative of human reasoning. Generalizations that described more complex forms of uncertainty quickly expanded within the discipline. The work of Turksen [2] on interval-valued stringent preferences has previously shown the usefulness of using intervals to convey the nuanced range of human judgment in fuzzy logic. This resulted in more general interval-valued frameworks [3, 4] whose non-membership degrees could be represented as ranges, allowing a better representation of imperfect information, and more specialized frameworks like Atanassov's intuitionistic fuzzy sets [5], which had a distinct non-membership degree to model hesitation. Combining these concepts to create hybrid frameworks was one of the most significant theoretical advances. Jun et al. [6] suggested cubic sets, which are interval-valued fuzzy sets plus fuzzy sets, to represent dual-characteristic information. Meanwhile, a radical and more comprehensive approach to neutrosophic sets whose properties were determined by the independent truth, indeterminacy, and falsity membership functions was provided by Smarandache's [7] neutrosophy. The development of interval neutrosophic sets [8], which limited such memberships to intervals within [0,1], validated the viability of this idea. The neutrosophic cubic set (NCS) was created by combining these two powerful ideas: cubic sets and neutrosophy. A powerful and adaptable tool that can handle multifarious uncertainty in three dimensions (T, I, and F) in both the interval and univariate forms is created by combining an interval neutrosophic set with a neutrosophic set, as defined by Jun et al. [9]. In order to manage this complex data structure with ease, additional research was conducted to build the theoretical underpinnings of NCS and novel set-theoretic operators as P-union and P-intersection [10]. However, this theoretical development's application to difficult real-world decision-making issues is what makes it truly valuable. The use of NCS in Multi-Criteria Decision Making (MCDM) has been the subject of extensive research as a result. In order to achieve this, researchers have developed a wide range of methods, including advanced aggregation operators like Dombi [11] operators and Einstein [12] operators to integrate the knowledge across two or more criteria, Grey Relational Analysis (GRA) [13] to rank alternatives, and similarity measures and cosine measures [14, 15] to compare alternatives. The literature's applications (such as those shown by Zhan et al. [16]) all support the idea that NCS is the most effective method for addressing the ambiguity, inconsistency, and incompleteness that characterize today's MCDM issues. Because of this literature, NCS is not only a theoretical interest but also a significant advancement in decision science mathematics.

1.1. Literature review

Broumi and Smarandache were pioneers in this sector. In a series of studies, they established and examined a number of basic neutrosophic set metrics. Broumi and Smarandache [17] established a basic toolkit for the new subject by proposing a number of similarity measurements of neutrosophic sets. By defining a correlation coefficient of INS, they generalized to Interval Neutrosophic Sets (INS), which define membership degrees by intervals rather than by precise numbers to indicate more uncertainty [18]. Furthermore, a cosine similarity measure of INS a traditional geometric notion adapted to the neutrosophic interval-value setting was developed by Broumi and Smarandache [19]. The period saw rapid advancement and sophistication. By investigating the dual concepts of similarity and entropy in neutrosophic sets and relating the degree of resemblance to the degree of uncertainty of the set as a whole, Majumder and Samanta [20] contributed to the theoretical backdrop. Ye [21] was particularly active; he proposed similarity measures of interval neutrosophic sets and integrated them into a useful MCDM technique, demonstrating a clear connection between theory and practice. In order to improve computing efficiency with real-world situations and a new generation of specialized similarity measures, simplified versions of neutrosophic sets, such as Single-Valued Neutrosophic Sets (SVNS) and Simplified Neutrosophic Sets (SNS), gained popularity. Another key figure was Ye [22], who suggested similarity measures of vectors on simplified neutrosophic sets and used them right away for MCDM problems. Additionally, by adapting the mathematical framework to the inadequacies of health care data, he improved the cosine similarity metrics to specific medical diagnoses [23].This was a broader medical orientation. Ye, Fu, and Ye [24] employed distance-based similarity measures in the same structures, both of which applied their models in medical diagnostics, while Ye et al. [25] used dice similarity measures in single-valued neutrophilic multisets. Its use was not restricted to the medical field; Ye [26] was able to apply a similarity measure based on cotangent functions to SVNS to steam turbine failure detection, indicating the instruments' suitability for use in an industrial setting. The implementation is the only way to properly understand these theoretical advancements. In the testing field of medical diagnostics, neutrosophic similarity assessments have taken center stage. In medical diagnostics, other researchers like Jafar et al. have made extensive use of fuzzy and soft set approaches. They are often based on Sanchez's approach, which uses tools like Intuitionistic Fuzzy Soft Matrices [27] and trapezoidal fuzzy numbers [28] and soft-set relations to characterize symptoms and diseases and produce diagnostic matches [29]. Despite having its roots in earlier fuzzy models, this literature demonstrates the application of similarity-based reasoning to important decision-making and acts as a standard by which the excellent performance of neutrosophic models (as demonstrated by Ye and others) can be measured. In the meantime, neutrosophic sets were discovered to be highly beneficial for image processing. In order to handle the noisy pixels, Cheng and Guo [30] presented a novel neutrosophic approach to image thresholding that is based on the idea of indeterminacy. Chen [31] described a comparison of similarity measures of fuzzy values and new approach to handling fuzzy decision-making problems [32]. Guo and Cheng [33], who expanded on this technique for picture segmentation a fundamental problem in computer vision replaced this and [34] described similarity measure between fuzzy sets and between elements. Their research demonstrated that more accurate and reliable segmentation was achievable by translating picture pixels into the neutrosophic domain, where ambiguous pixels may have been those on the border between areas. Table 1 below lists references that highlight real-world problems with the research's applicability.

Table 1: From drone swarms to cybersecurity: the use of neutrosophic models in contemporary military operations

Model	**Components**	**Handling Contradiction**	**Best Military Application Domain**
SVNS [35]	$T/I/F \in [0,1]$	Basic	Cyber security threat scoring
IVNSS [36]	Interval-valued T/I/F	Moderate NATO adoption barriers	Boarder surveillance system
Neutrosophic Classifier [37]	T/I/F decision boundaries	High	Deception detection(92 % accuracy)
Battlefield Algorithm [38, 39]	Aggregated T/I/F parameters	Very High	Troop deployment planning
QNSS [40]	T/C/U/F quadri-partitioned	Extreme	Counter-terrorism intelligence analysis
Neutrosophic NN [41]	Neutral-adapted T/I/F nodes	High	Radar signal interpretation
Drone response System [42]	Dynamic T/I/F optimization	Very High	Multi-drone threat coordination
Implementation Challenges [43]	NATO adoption barriers	Computational/ training hurdles	Military deployment

Table 1 further demonstrates that RNS and RNSS have several significant differences, such as contradicting modeling and granularity but no DVN. Although DVNSS can effectively operate DVN, its features, including closure and continuity, are not scalable. Because of its high computational complexity (O(n 4)), QNSS can effectively handle contradictions, which effectively makes real-time applications impossible. Due to their lack of topographical or local reasoning, the models' inability to simulate boundary behavior at the border between ranges is a shortcoming. In the same vein, Table 1 lists the many potentially beneficial but unfinished military applications of neutrosophic frameworks, such as deception detection and radar interpretation. The majority of models are only suitable for decision scoring; they lack geometric or visual interpretation, making them difficult to integrate into a human in the loop system.

Despite its potential, models like the Drone Response System and the Neutosophic Neural Network do not make use of statistical models like Heatmaps or more sophisticated models like PCA or t-SNE. There is currently no contemporary visual analytics that combines topological operators with quadri-partitioned neutrosophic reasoning on high-dimensional defense metrics data. This study was conducted primarily to fill these gaps. By offering a new theoretical framework that complements quadri partitioned neutrosophic soft sets with soft topological structures, as well as by introducing cosine similarity measurements and visual analysis tools, this study can try to address the operational and interpretive shortcomings that can be found in both tables. It offers a computationally realistic, mathematically sound, and visually pleasing solution to real-world scenario operations like classifying military targets in an unpredictable environment. The investigation of supra open soft sets and its various decompositions and applications, as well as soft set theory, are both superseded by supra soft topology, according to the sources provided. Fundamental results on decompositions of supra soft sets, together with the concept of soft continuity in this context, were provided by El-Sheikh and Abd Ellatif's basic contributions [44]. Supra soft strongly generalized closed sets [45], supra soft strongly extra generalized closed sets [46], and supra soft strongly semi* generalized closed sets [47] are only a few of the specific classes of soft sets that are now being studied in this field. Furthermore, the ideas have been crucial in defining and researching different forms of soft connectedness [48] as well as related soft separation axioms [49][50][51]. The research of supra soft compactness [52] and interactions with soft ideals [53] have also contributed to the development of the theory.

1.2. Research Gap

There are several gaps even though this study establishes the foundation for the quadri-partition neutrosophic soft locally compact spaces (QPNSLCS) and shows how they can be used for clustering and dimensionality reduction. First, the theoretical results are limited to local compactness on Hausdorff condition, and the response of QPNSLCS to more generalized topological contexts and weaker separation axioms is still unclear. Second, QPNSLCS has not yet been fully integrated into practice; its applicability in engineering, medical diagnostics, artificial intelligence, and decision-making has not been proven. Third, there is a gap between data science theory and reality because the computational examples are based on illustrative approaches (t-SNE, PCA, UMAP, and ICA) that have not been thoroughly empirically tested on big or domain-specific data. Finally, the issue of distortions in signal recovery using ICA shows that the algorithm's robustness and mathematical models need to be strengthened. Closing these gaps will facilitate the conversion of QPNSLCS's theoretical implications into more significant practical ones.

1.3. Novelty

In order to extend the mathematical framework of uncertainty management in complex topological structures, the study introduces quadri-partition neutrosophic soft locally compact spaces (QPNSLCS), a unique extension of quadri-partition neutrosophic soft topological spaces (QPNSTS). It demonstrates that compact neighborhoods and subspaces are guaranteed by local compactness with the Hausdorff condition, providing a stronger theoretical foundation than the current neutrosophic and soft topological models. Combining the theoretical framework with dimensionality reduction and clustering methods (t-SNE, PCA, UMAP, and ICA) enables the real data analysis to be added to the abstract mathematics, allowing for a deeper comprehension of how to analyze high-dimensional data.

2. Preliminaries

This segment addresses the basic functions.
To begin with, the idea of neutrosophic soft sets was first established by Maji [54]. Later, Deli and Bromi [55] refined and modified this concept, as detailed below:

Definition 1. *$\acute{E}$ represents a collection of parameters and $\mathcal{M}$ be an initial universe set. $P(\mathcal{M})$ denotes the set of all NSSs for $\mathcal{M}$. A set defined by a set-valued function $\tilde{\mathcal{L}}$ that represents a mapping of the form $\tilde{\mathcal{L}} : \acute{E} \to P(\mathcal{M})$ is called NSS $(\tilde{\mathcal{L}}, \acute{E})$ over $\mathcal{M}$, with $\tilde{\mathcal{L}}$ being an approximate function of the NSS $(\tilde{\mathcal{L}}, \acute{E})$. In other terms, the NSS can be described as a set of ordered pairs,*

$$(\tilde{\mathcal{L}}, \acute{E}) = \left\{ \Big(e, \langle x, T_{\tilde{\mathcal{L}}(e)}(x), I_{\tilde{\mathcal{L}}(e)}(x), F_{\tilde{\mathcal{L}}(e)}(x) \rangle : x \in \mathcal{M} \Big) : e \in \acute{E} \right\}.$$

$T_{\tilde{\mathcal{L}}(e)}(x)$, $I_{\tilde{\mathcal{L}}(e)}(x)$, $F_{\tilde{\mathcal{L}}(e)}(x) \in [0,1]$ are the truth, indeterminacy, and falsity-membership functions of $\tilde{\mathcal{L}}(e)$, respectively, all of which lie within the interval $[0,1]$. The inequality

$$0 \le T_{\tilde{\mathcal{L}}(e)}(x) + I_{\tilde{\mathcal{L}}(e)}(x) + F_{\tilde{\mathcal{L}}(e)}(x) \le 3$$

is clear since the supremum of each T, I, and F is 1.

Definition 2. *[56] Let $(\tilde{\mathcal{L}}, \acute{E})$ be NSS. $(\tilde{\mathcal{L}}, \acute{E})^c$ is the complement of $(\tilde{\mathcal{L}}, \acute{E})$:*

$$(\tilde{\mathcal{L}}, \acute{E})^c = \left\{ \left(e, \langle x, F_{\tilde{\mathcal{L}}(e)}(x), 1 - I_{\tilde{\mathcal{L}}(e)}(x), T_{\tilde{\mathcal{L}}(e)}(x) \rangle : x \in \mathcal{M} \right) : e \in \acute{E} \right\}.$$

Obvious that:

$$\left((\tilde{\mathcal{L}}, \acute{E})^c \right)^c = (\tilde{\mathcal{L}}, \acute{E}).$$

Definition 3. *[57] Let $(\tilde{\mathcal{L}}, \acute{E})$ and $(\tilde{\mathfrak{J}}, \acute{E})$ be two NSSs. $(\tilde{\mathcal{L}}, \acute{E}) \tilde{\subseteq} (\tilde{\mathfrak{J}}, \acute{E})$ if:*

$$T_{\tilde{\mathcal{L}}(e)}(x) \leq T_{\tilde{\mathfrak{J}}(e)}(x), \quad I_{\tilde{\mathcal{L}}(e)}(x) \leq I_{\tilde{\mathfrak{J}}}(e)(x), \quad F_{\tilde{\mathcal{L}}(e)}(x) \geq F_{\tilde{\mathfrak{J}}(e)}(x), \quad \forall e \in \acute{E}, \forall x \in \mathcal{M}.$$

Definition 4. *[57] Let $(\tilde{\mathcal{L}}_1, \acute{E})$ and $(\tilde{\mathcal{L}}_2, \acute{E})$ be two NSSs. Then union of these sets is denoted by $(\tilde{\mathcal{L}}_1, \acute{E}) \cup (\tilde{\mathcal{L}}_2, \acute{E}) = (\tilde{\mathcal{L}}_3, \acute{E})$ with:*

$$(\tilde{\mathcal{L}}_3, \acute{E}) = \left\{ \left(e, \langle x, T_{\tilde{\mathcal{L}}_{3(e)}}(x), I_{\tilde{\mathcal{L}}_{3(e)}}(x), F_{\tilde{\mathcal{L}}_{3(e)}}(x) \rangle : x \in \mathcal{M} \right) : e \in \acute{E} \right\}.$$

Where:

$$\begin{cases} T_{\tilde{\mathcal{L}}_{3(e)}}(x) & = \max\{T_{\tilde{\mathcal{L}}_{1(e)}}(x), T_{\tilde{\mathcal{L}}_{2(e)}}(x)\}, \\ I_{\tilde{\mathcal{L}}_{3(e)}}(x) & = \max\{I_{\tilde{\mathcal{L}}_{1(e)}}(x), I_{\tilde{\mathcal{L}}_{2(e)}}(x)\}, \\ F_{\tilde{\mathcal{L}}_{3(e)}}(x) & = \min\{F_{\tilde{\mathcal{L}}_{1(e)}}(x), F_{\tilde{\mathcal{L}}_{2(e)}}(x)\}. \end{cases}$$

Definition 5. *[57] Let $(\tilde{\mathcal{L}}_1, \acute{E})$ and $(\tilde{\mathcal{L}}_2, \acute{E})$ be two NSSs. Then intersection of these two sets is symbolized by $(\tilde{\mathcal{L}}_1, \acute{E}) \cap (\tilde{\mathcal{L}}_2, \acute{E}) = (\tilde{\mathcal{L}}_3, \acute{E})$ with:*

$$(\tilde{\mathcal{L}}_3, \acute{E}) = \left\{ \left(e, \langle x, T_{\tilde{\mathcal{L}}_{3(e)}}(x), I_{\tilde{\mathcal{L}}_{3(e)}}(x), F_{\tilde{\mathcal{L}}_{3(e)}}(x) \rangle : x \in \mathcal{M} \right) : e \in \acute{E} \right\}.$$

Where:

$$\begin{cases} T_{\tilde{\mathcal{L}}_{3(e)}}(x) & = \min\{T_{\tilde{\mathcal{L}}_{1(e)}}(x), T_{\tilde{\mathcal{L}}_{2(e)}}(x)\}, \\ I_{\tilde{\mathcal{L}}_{3(e)}}(x) & = \min\{I_{\tilde{\mathcal{L}}_{1(e)}}(x), I_{\tilde{\mathcal{L}}_{2(e)}}(x)\}, \\ F_{\tilde{\mathcal{L}}_{3(e)}}(x) & = \max\{F_{\tilde{\mathcal{L}}_{1(e)}}(x), F_{\tilde{\mathcal{L}}_{2(e)}}(x)\}. \end{cases}$$

Definition 6. *[57] Let $(\tilde{\mathcal{L}}_1, \acute{E})$ and $(\tilde{\mathcal{L}}_2, \acute{E})$ be two NSSs. Then $(\tilde{\mathcal{L}}_1, \acute{E}) \setminus (\tilde{\mathcal{L}}_2, \acute{E})$ is denoted by $(\tilde{\mathcal{L}}_1, \acute{E}) \setminus (\tilde{\mathcal{L}}_2, \acute{E}) = (\tilde{\mathcal{L}}_3, \acute{E})$ and is defined by:*

$$(\tilde{\mathcal{L}}_3, \acute{E}) = \left\{ \left(e, \langle x, T_{\tilde{\mathcal{L}}_{3(e)}}(x), I_{\tilde{\mathcal{L}}_{3(e)}}(x), F_{\tilde{\mathcal{L}}_{3(e)}}(x) \rangle : x \in \mathcal{M} \right) : e \in \acute{E} \right\}.$$

Where:

$$\begin{cases} T_{\tilde{\mathcal{L}}_{3(e)}}(x) & = \min\{T_{\tilde{\mathcal{L}}_{1(e)}}(x), T_{\tilde{\mathcal{L}}_{2(e)}}(x)\}, \\ I_{\tilde{\mathcal{L}}_{3(e)}}(x) & = \min\{I_{\tilde{\mathcal{L}}_{1(e)}}(x), I_{\tilde{\mathcal{L}}_{2(\acute{e})}}(x)\}, \\ F_{\tilde{\mathcal{L}}_{3(e)}}(x) & = \max\{F_{\tilde{\mathcal{L}}_{1(e)}}(x), F_{\tilde{\mathcal{L}}_{2(e)}}(x)\}. \end{cases}$$

Definition 7. *[57] 1. A NSS $(\tilde{\mathcal{L}}, \acute{E})$ is said to be a null NSS if:*

$$T_{\tilde{\mathcal{L}}(e)}(x) = 0, \quad I_{\tilde{\mathcal{L}}(e)}(x) = 0, \quad F_{\tilde{\mathcal{L}}(e)}(x) = 1, \quad \forall e \in \acute{E}, \forall x \in \mathcal{M}.$$

It is denoted by $0_{(\mathcal{M}, \acute{E})}$.

2. A NSS $(\tilde{\mathcal{L}}, \acute{E})$ is said to be an absolute NSS if:

$$T_{\tilde{\mathcal{L}}(e)}(x) = 1, \quad I_{\tilde{\mathcal{L}}(e)}(x) = 1, \quad F_{\tilde{\mathcal{L}}(e)}(x) = 0, \quad \forall e \in \acute{E}, \forall x \in \mathcal{M}.$$

It is symbolized as $1_{(\mathcal{M}, \acute{E})}$.

$$0_{(\mathcal{M}, \acute{E})} = 1_{(\mathcal{M}, \acute{E})}, \quad 1_{(\mathcal{M}, \acute{E})} = 0_{(\mathcal{M}, \acute{E})}.$$

is obvious.

Definition 8. *[58]$\acute{E}$ be the collection of parameters and $\mathcal{M}$ denotes an initial universe set. $P(\mathcal{M})$ denotes the set of all NSs for $\mathcal{M}$. A set defined by a set valued function $\tilde{\mathcal{L}}$ that represents a mapping of the form $\tilde{\mathcal{L}} : \acute{E} \to P(\mathcal{M})$ is called QPNSS $(\tilde{\mathcal{L}}, \acute{E})$ over $\mathcal{M}$, with $\tilde{\mathcal{L}}$ being an appropriate function of this NSS. In other terms, the QPNSS can be described as a set of ordered pairs,*

$$(\tilde{\mathcal{L}}, \acute{E}) = \left\{ \left(e, \langle x, AbT_{\tilde{\mathcal{L}}(e)}(x), ReT_{\tilde{\mathcal{L}}(e)}(x), ReF_{\tilde{\mathcal{L}}(e)}(x), AbF_{\tilde{\mathcal{L}}(e)}(x) \rangle : x \in \mathcal{M} \right) : e \in \acute{E} \right\}.$$

$AbT_{\tilde{\mathcal{L}}(e)}(s)$, $ReT_{\tilde{\mathcal{L}}(e)}(s)$, $ReF_{\tilde{\mathcal{L}}(e)}(s)$, $AbF_{\tilde{\mathcal{L}}(e)}(s) \in [0,1]$ are the truth, relative truth, relative false, and false-membership functions of $\tilde{\mathcal{L}}(e)$, respectively, all of which lie within the interval $[0,1]$. The inequality

$$0 \leq AbT_{\tilde{\mathcal{L}}(e)}(s) + ReT_{\tilde{\mathcal{L}}(e)}(s) + ReF_{\tilde{\mathcal{L}}(e)}(s) + AbF_{\tilde{\mathcal{L}}(e)}(s) \leq 4.$$

is clear since the supremum of each T, I, and F is 1.

Definition 9. *[58]The complement of QPNSS $(\tilde{\mathcal{L}}, \acute{E})$ is denoted by $(\tilde{\mathcal{L}}, \acute{E})^c$ and is given as follows:*

$$(\tilde{\mathcal{L}}, \acute{E})^c = \left\{ \left(e, \langle x, AbF_{\tilde{\mathcal{L}}(e)}(x), ReF_{\tilde{\mathcal{L}}(e)}(x), ReT_{\tilde{\mathcal{L}}(e)}(x), AbT_{\tilde{\mathcal{L}}(e)}(x) \rangle : x \in \mathcal{M} \right) : e \in \acute{E} \right\}.$$

Definition 10. *[58]$(\tilde{\mathcal{L}}, \acute{E})$ is subset of $(\tilde{\mathfrak{J}}, \acute{E})$ if*

$$\begin{aligned} AbT_{\tilde{\mathcal{L}}(e)}(x) &\leq AbT_{\tilde{\mathfrak{J}}(e)}(x), \\ ReT_{\tilde{\mathcal{L}}(e)}(x) &\leq ReT_{\tilde{\mathfrak{J}}(e)}(x), \\ ReF_{\tilde{\mathcal{L}}(e)}(x) &\geq ReF_{\tilde{\mathfrak{J}}(e)}(x), \\ AbF_{\tilde{\mathcal{L}}(e)}(x) &\geq AbF_{\tilde{\mathfrak{J}}(e)}(x), \end{aligned}$$

for all $e \in \acute{E}$ and $x \in \mathcal{M}$.

Definition 11. *[58]The union of two QPNSSs $(\tilde{\mathcal{L}}, \acute{E})$ and $(\tilde{\mathfrak{J}}, \acute{E})$ is denoted by $(\tilde{\mathcal{L}}, \acute{E}) \cup (\tilde{\mathfrak{J}}, \acute{E}) = (\tilde{H}, \acute{E})$ with:*

$$(\tilde{H}, \acute{E}) = \left\{ \left(e, \langle x, AbT_{\tilde{H}(e)}(x), ReT_{\tilde{H}(e)}(x), ReF_{\tilde{H}(e)}(x), AbF_{\tilde{H}(e)}(x) \rangle : x \in \mathcal{M} \right) : e \in \acute{E} \right\}.$$

Where

$$\begin{aligned} AbT_{\tilde{H}(e)}(x) &= \max \left\{ AbT_{\tilde{\mathcal{L}}(e)}(x), AbT_{\tilde{\mathfrak{J}}(e)}(x) \right\}, \\ ReT_{\tilde{H}(e)}(x) &= \max \left\{ ReT_{\tilde{\mathcal{L}}(e)}(x), ReT_{\tilde{\mathfrak{J}}(e)}(x) \right\}, \\ ReF_{\tilde{H}(e)}(x) &= \min \left\{ ReF_{\tilde{\mathcal{L}}(e)}(x), ReF_{\tilde{\mathfrak{J}}(e)}(x) \right\}, \\ AbF_{\tilde{H}(e)}(x) &= \min \left\{ AbF_{\tilde{\mathcal{L}}(e)}(x), AbF_{\tilde{\mathfrak{J}}(e)}(x) \right\}. \end{aligned}$$

Definition 12. *[58]The intersection of two QPNSSs $(\tilde{\mathcal{L}}, \acute{E})$ and $(\tilde{\mathfrak{J}}, \acute{E})$ is denoted by $(\tilde{\mathcal{L}}, \acute{E}) \cap (\tilde{\mathfrak{J}}, \acute{E}) = (\tilde{H}, \acute{E})$ and is given as:*

$$(\tilde{H}, \acute{E}) = \left\{ \left(e, \langle x, AbT_{\tilde{H}(e)}(x), ReT_{\tilde{H}(e)}(x), ReF_{\tilde{H}(e)}(x), AbF_{\tilde{H}(e)}(x) \rangle : x \in \mathcal{M} \right) : e \in \acute{E} \right\}.$$

Where

$$AbT_{\tilde{H}(e)}(x) = \min \left\{ AbT_{\tilde{\mathcal{L}}(e)}(x), AbT_{\tilde{\mathfrak{J}}(e)}(x) \right\},$$

$$ReT_{\tilde{H}(e)}(x) = \min\left\{ReT_{\tilde{\mathcal{L}}(e)}(x), ReT_{\tilde{\mathfrak{J}}(e)}(x)\right\},$$
$$ReF_{\tilde{H}(e)}(x) = \max\left\{ReF_{\tilde{\mathcal{L}}(e)}(x), ReF_{\tilde{\mathfrak{J}}(e)}(x)\right\},$$
$$AbF_{\tilde{H}(e)}(x) = \max\left\{AbF_{\tilde{\mathcal{L}}(e)}(x), AbF_{\tilde{\mathfrak{J}}(e)}(x)\right\}.$$

Definition 13. *[58]The difference of two QPNSSs $(\tilde{\mathcal{L}}, \acute{E})$ and $(\tilde{\mathfrak{J}}, \acute{E})$ is denoted by $(\tilde{H}, \acute{E}) = (\tilde{\mathcal{L}}, \acute{E}) \cap (\tilde{\mathfrak{J}}, \acute{E})^c$ and is given as:*

$$(\tilde{H}, \acute{E}) = \left\{\left(e, \langle x, AbT_{\tilde{H}(e)}(x), ReT_{\tilde{H}(e)}(x), ReF_{\tilde{H}(e)}(x), AbF_{\tilde{H}(e)}(x)\rangle\right) : x \in \mathcal{M}, e \in \acute{E}\right\}.$$

Where

$$AbT_{\tilde{H}(e)}(x) = \min\left\{AbT_{\tilde{\mathcal{L}}(e)}(x), AbT_{\tilde{\mathfrak{J}}(e)}(x)\right\},$$
$$ReT_{\tilde{H}(e)}(x) = \min\left\{ReT_{\tilde{\mathcal{L}}(e)}(x), ReT_{\tilde{\mathfrak{J}}(e)}(x)\right\},$$
$$ReF_{\tilde{H}(e)}(x) = \max\left\{ReF_{\tilde{\mathcal{L}}(e)}(x), ReF_{\tilde{\mathfrak{J}}(e)}(x)\right\},$$
$$AbF_{\tilde{H}(e)}(x) = \max\left\{AbF_{\tilde{\mathcal{L}}(e)}(x), AbF_{\tilde{\mathfrak{J}}(e)}(x)\right\}.$$

Definition 14. *[58]If the family of QPNSSs is $\{(\tilde{\mathcal{L}}_i, \acute{E}) : i \in I\}$. Then,*

$$\bigcup_{i\in I}(\tilde{\mathcal{L}}_i, \acute{E}) = \left\{\left(e, \langle x, \sup_{i\in I} AbT_{\tilde{\mathcal{L}}_{i(e)}}(x), \sup_{i\in I} ReT_{\tilde{\mathcal{L}}_{i(e)}}(x), \inf_{i\in I} ReF_{\tilde{\mathcal{L}}_{i(e)}}(x), \inf_{i\in I} AbF_{\tilde{\mathcal{L}}_{i(e)}}(x)\rangle\right) : x \in \mathcal{M}, e \in \acute{E}\right\}.$$

$$\bigcap_{i\in I}(\tilde{\mathcal{L}}_i, \acute{E}) = \left\{\left(e, \langle x, \inf_{i\in I} AbT_{\tilde{\mathcal{L}}_{i(e)}}(x), \inf_{i\in I} ReT_{\tilde{\mathcal{L}}_{i(e)}}(x), \sup_{i\in I} ReF_{\tilde{\mathcal{L}}_{i(e)}}(x), \sup_{i\in I} AbF_{\tilde{\mathcal{L}}_{i(e)}}(x)\rangle\right) : x \in \mathcal{M}, e \in \acute{E}\right\}.$$

Definition 15. *[58]If QPNSSs $(\tilde{\mathcal{L}}, \acute{E})$, $(\tilde{\mathfrak{J}}, \acute{E})$ on $\mathcal{M}$ are given. Then, the "AND" operation on them is denoted by $(\tilde{\mathcal{L}}, \acute{E}) \wedge (\tilde{\mathfrak{J}}, \acute{E}) = (\tilde{H}, \acute{E} \times \acute{E})$ with:*

$$(\tilde{H}, \acute{E} \times \acute{E}) = \left\{\left((e_1, e_2), \langle x, AbT_{\tilde{H}}(e_1, e_2)(x), ReT_{\tilde{H}}(e_1, e_2)(x),\right.\right.$$
$$\left.\left. ReF_{\tilde{H}}(e_1, e_2)(x), AbF_{\tilde{H}}(e_1, e_2)(x) : x \in \mathcal{M}\rangle\right) : (e_1, e_2) \in \acute{E} \times \acute{E}\right\}.$$

Where

$$AbT_{\tilde{H}(e)}(x) = \min\left\{AbT_{\tilde{\mathcal{L}}(e)}(x), AbT_{\tilde{\mathfrak{J}}(e)}(x)\right\},$$
$$ReT_{\tilde{H}(e)}(x) = \min\left\{ReT_{\tilde{\mathcal{L}}(e)}(x), ReT_{\tilde{\mathfrak{J}}(e)}(x)\right\},$$
$$ReF_{\tilde{H}(e)}(x) = \max\left\{ReF_{\tilde{\mathcal{L}}(e)}(x), ReF_{\tilde{\mathfrak{J}}(e)}(x)\right\},$$
$$AbF_{\tilde{H}(e)}(x) = \max\left\{AbF_{\tilde{\mathcal{L}}(e)}(x), AbF_{\tilde{\mathfrak{J}}(e)}(x)\right\}.$$

Definition 16. *[58]If QPNSSs $(\tilde{\mathcal{L}}, \acute{E})$, $(\tilde{\mathfrak{J}}, \acute{E})$ on $\mathcal{M}$ are given. Then, the "OR" operation on them is denoted by $(\tilde{\mathcal{L}}, \acute{E}) \vee (\tilde{\mathfrak{J}}, \acute{E}) = (\tilde{H}, \acute{E} \times \acute{E})$ with:*

$$(\tilde{H}, \acute{E} \times \acute{E}) = \left\{\left((e_1, e_2), \langle x, AbT_{\tilde{H}(e_1,e_2)}(x), ReT_{\tilde{H}(e_1,e_2)}(x),\right.\right.$$
$$\left.\left. ReF_{\tilde{H}(e_1,e_2)}(x), AbF_{\tilde{H}(e_1,e_2)}(x) : x \in \mathcal{M}\rangle\right) : (e_1, e_2) \in \acute{E} \times \acute{E}\right\}.$$

Where

$$\begin{aligned}
AbT_{\tilde{H}(e)}(x) &= \max\left\{AbT_{\tilde{\mathcal{L}}(e)}(x), AbT_{\tilde{\mathfrak{J}}(e)}(x)\right\},\\
ReT_{\tilde{H}(e)}(x) &= \max\left\{ReT_{\tilde{\mathcal{L}}(e)}(x), ReT_{\tilde{\mathfrak{J}}(e)}(x)\right\},\\
ReF_{\tilde{H}(e)}(x) &= \min\left\{ReF_{\tilde{\mathcal{L}}(e)}(x), ReF_{\tilde{\mathfrak{J}}(e)}(x)\right\},\\
AbF_{\tilde{H}(e)}(x) &= \min\left\{AbF_{\tilde{\mathcal{L}}(e)}(x), AbF_{\tilde{\mathfrak{J}}(e)}(x)\right\}.
\end{aligned}$$

Definition 17. *[58]Let the be the family of all QPNSSs is QPNSS $(\mathcal{M}, \acute{E})$. If $\tau \subset QPNSS(\mathcal{M}, \acute{E})$, then τ is a QPNST on $\mathcal{M}$ if:*

(i) $0_{(\mathcal{M},\acute{E})}, 1_{(\mathcal{M},\acute{E})} \in \tau$,

(ii) The union of any number of QPNSSs in τ belongs to τ,

(iii) The intersection of a finite number of QPNSSs in τ belongs to τ.

Then, $(\mathcal{M}, \tau, \acute{E})$ is QPNSTS over $\mathcal{M}$.

3. Local Compactness in Quadri-Partition Neutrosophic Soft Topological Space

Quadri-partition neutrosophic soft locally compact space is introduced in this section. It illustrates how local compactness, particularly when combined with the Hausdorff condition, guarantees compact neighborhoods and maintains compactness in subspaces. The notion of approaching uncertainty of complex topological structures is supported by these results.

Definition 18. *$(\mathcal{M}, \tau^{QPNSS}, \hat{E})$ is QPNSTS.$(\mathcal{M}, \tau^{QPNSS}, \hat{E})$ is said to be QPNSLCS if for $x^e_{(r_1,r_2,r_3,r_4)} \in QPNSS(\tilde{\mathcal{L}}, \hat{E})$, $\exists QPNSN(\mathrm{U}, \hat{E}) \in \tau^{QPNSS}$ of $x^e_{(r_1,r_2,r_3,r_4)}$ with $QPNSC\overline{(\tilde{\mathrm{U}}, \hat{E})}$. When $(\mathcal{M}, \tau^{QPNSS}, \hat{E})$ is also QPNSH.*

Theorem 1. *If $(\mathcal{M}, \tau^{QPNSS}, \hat{E})$ is QPNSTLC and QPNSH, $(f, \hat{E}) \in QPNSS(\mathcal{M}, \hat{E})$ QPNSCS and $(f, \hat{E})\tilde{\subseteq}(\mathrm{V}, \hat{E})$, $(\mathrm{V}, \hat{E}) \in \tau^{QPNSS}$ then $\exists(\mathrm{U}, \hat{E}) \in \tau^{QPNSS}$ s.t. $\overline{(\mathrm{U}, \hat{E})}$ is QPNSC also $(f, \hat{E})\tilde{\subseteq}(\mathrm{U}, \hat{E})\tilde{\subseteq}\overline{(\mathrm{U}, \hat{E})}\tilde{\subseteq}(\mathrm{V}, \hat{E})$.*

Proof. Since $(\mathcal{M}, \tau^{QPNSS}, \hat{E})$ is QPNSH, $\exists(\mathrm{V}, \hat{E})_{x^e_{(r_1,r_2,r_3,r_4)}}$ nbhd for $x^e_{(r_1,r_2,r_3,r_4)} \in (f, \hat{E})\tilde{\subseteq}(\mathrm{V}, \hat{E})$, s.t.

$$x^e_{(\alpha,\beta,\gamma)} \in (\mathrm{V}, \hat{E})_{x^e_{(r_1,r_2,r_3,r_4)}}\tilde{\subseteq}\overline{(\mathrm{V}, \hat{E})_{x^e_{(r_1,r_2,r_3,r_4)}}}\tilde{\subseteq}(\mathrm{V}, \hat{E}).$$

Since $(\mathcal{M}, \tau^{QPNSS}, \hat{E})$ is QPNSLCS, each $x^e_{(r_1,r_2,r_3,r_4)} \in (\mathrm{V}, \hat{E})$ has a $\overline{(\mathcal{W}, \hat{E})_{x^e_{(r_1,r_2,r_3,r_4)}}}$ compact nbhd. Therefore the nbhd of

$$(\mathrm{U}, \hat{E})_{x^e_{(\alpha,\beta,\gamma)}} = (\mathrm{V}, \hat{E})_{x^e_{(r_1,r_2,r_3,r_4)}} \cap (\mathrm{V}, \hat{E})_{x^e_{(r_1,r_2,r_3,r_4)}}$$

of $x^e_{(r_1,r_2,r_3,r_4)}\overline{(\mathrm{U}, \hat{E})_{x^e_{(r_1,r_2,r_3,r_4)}}}$ is compact, since it is $(\subset ss\tilde{\subseteq})\overline{(\mathcal{W}, \hat{E})_{x^e_{(r_1,r_2,r_3,r_4)}}}$. Since QPNSS $(f, \hat{E})$ compact, $\{(\mathrm{U}, \hat{E})_{x^e_{(r_1,r_2,r_3,r_4)}}\}_{x^e_{(r_1,r_2,r_3,r_4)} \in (f,\hat{E})}$ QPNS cover of $(f, \hat{E})$ has a finite $(\mathrm{U}, \hat{E})_{1x^e_{(r_1,r_2,r_3,r_4)}}, ..., (\mathrm{U}, \hat{E})_{nx^e_{(r_1,r_2,r_3,r_4)}}$ QPNS sub-cover.
Here, for open set $(U, E) = \bigcup_{i=1}^{n}(\mathrm{U}, \hat{E})_{x^e_{(r_1,r_2,r_3,r_4)}}$.

$$(f, \hat{E})\tilde{\subseteq}(\mathrm{U}, \hat{E})\tilde{\subseteq}\overline{(\mathrm{U}, \hat{E})} = \bigcup_{i=1}^{n}\overline{(\mathrm{U}, \hat{E})_{x^e_{(r_1,r_2,r_3,r_4)}}}\tilde{\subseteq}\bigcup_{i=1}^{n}\overline{(\mathrm{U}, \hat{E})_{x^e_{(r_1,r_2,r_3,r_4)}}}\tilde{\subseteq}(\mathrm{V}, \hat{E}).$$

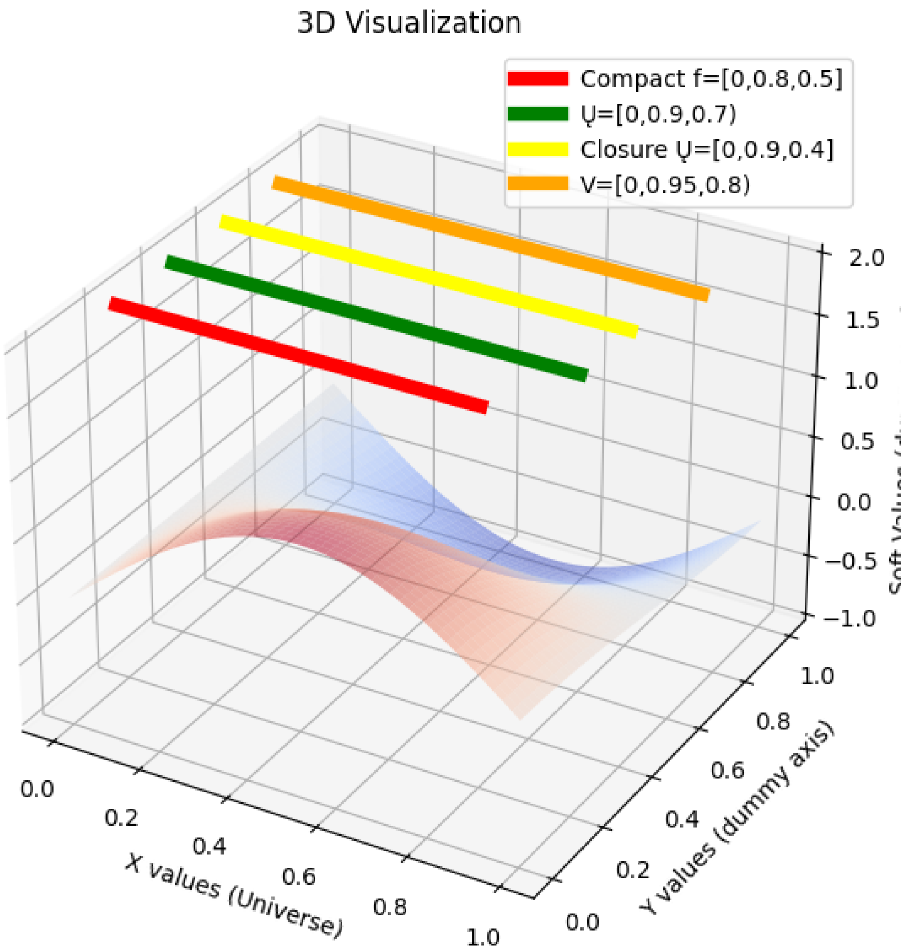

Figure 1

Theorem 2. *If* $(\mathcal{M}, \tau^{QPNSS}, \hat{E})$ *is QPNSTLC and QPNSH,* $(f, \hat{E}) \in QPNSS(\mathcal{M}, \hat{E})$ *QPNS closed (open) set, then* $((f, \hat{E}), \tau^{QPNSS}_{(f,\hat{E})}\hat{E})$ *is QPNSLC.*

Proof. Let $(\mathcal{M}, \tau^{QPNSS}, \hat{E})$ is QPNSTLCHS and $(f, \hat{E}) \in QPNSS(\mathcal{M}, \hat{E})$ be a QPNS closed set. Consider compact neighborhood $\overline{(\mathrm{U}, \hat{E})}$ of each $x^e_{(r_1,r_2,r_3,r_4)}(f, \hat{E}) \in (\mathcal{M}, \tau^{QPNSS}, \hat{E})$. For open neighborhood of $x^e_{(r_1,r_2,r_3,r_4)}(\mathrm{U}, \hat{E}) \cap (f, \hat{E})$ in $((f, \hat{E}), \tau^{QPNSS}_{(f,\hat{E})}\hat{E})$, $\overline{(\mathrm{U}, \hat{E})} \cap (f, \hat{E})$ is compact because it is

$$\overline{(\mathrm{U}, \hat{E}) \cap (f, \hat{E})} = \overline{(\mathrm{U}, \hat{E})} \cap (f, \hat{E}) \tilde{\subseteq} \overline{(\mathrm{U}, \hat{E})}.$$

that is $((f, \hat{E}), \tau^{QPNSS}_{(f,\hat{E})}\hat{E})$ is QPNSLCHS. When we make the proof for QPNS closed set, $(\mathcal{M}, \tau^{QPNSS}, \hat{E})$ does not need to be a QPNSHS. Now, let $(f, \hat{E}) \in QPNSS(\mathcal{M}, \hat{E})$ be a QPNSO. Since the single-point set in QPNSHS is QPNSC, $(\mathrm{U}, \hat{E}) \in \tau^{QPNSS}$ is present so that

$$x^e_{(r_1,r_2,r_3,r_4)} \tilde{\subseteq} (\mathrm{U}, \hat{E}) \tilde{\subseteq} \overline{(\mathrm{U}, \hat{E})} \tilde{\subseteq} (f, \hat{E}), (\mathrm{U}, \hat{E}).$$

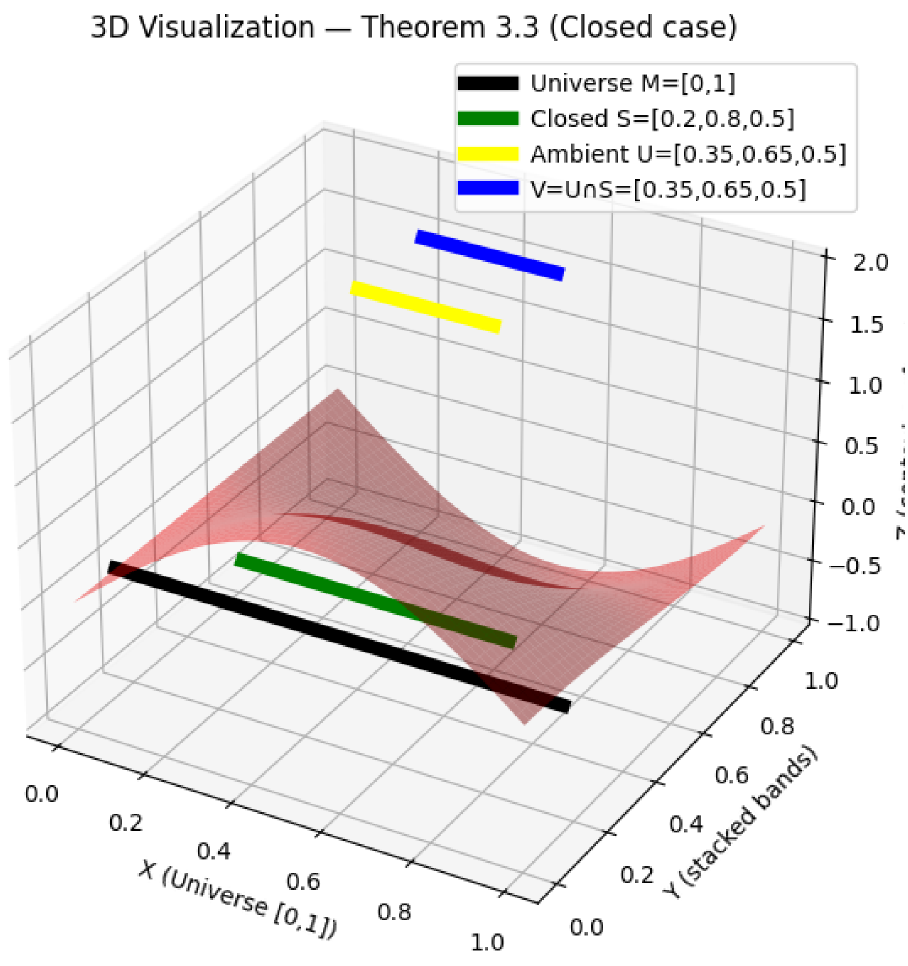
3D Visualization — Theorem 3.3 (Closed case)
Universe M=[0,1]
Closed S=[0.2,0.8,0.5]
Ambient U=[0.35,0.65,0.5]
V=U∩S=[0.35,0.65,0.5]
X (Universe [0,1])
Y (stacked bands)
0.0
0.2
0.4
0.6
0.8
1.0
2.0
1.5
1.0
0.5
0.0
−0.5
−1.0

Figure 2

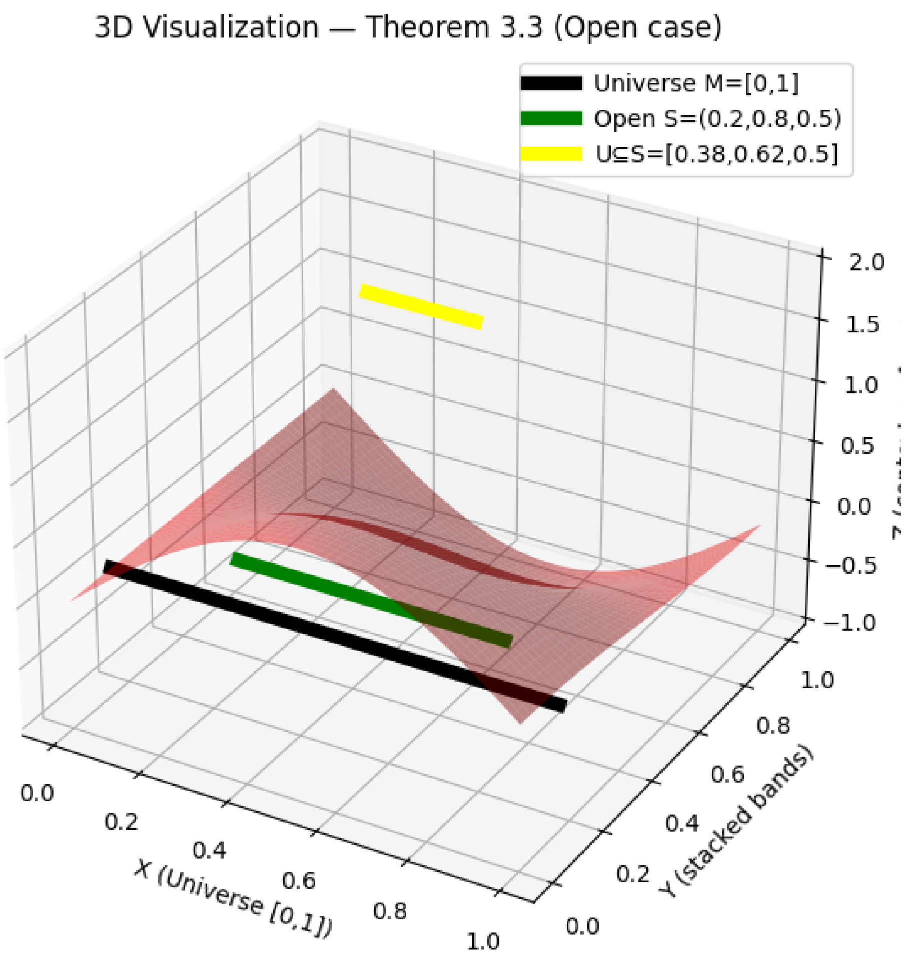

Figure 3

4. A Statistical and Machine Learning Framework for Target Identification in Defense Applications

One analytical technique for determining the degree of similarity between two vectors (data) is the tangent similarity measure (TSM). It is widely used in a variety of machine learning, image processing, and data analysis applications. By taking into account the geometric orientation of the data points, TSM will be able to uncover hidden patterns and associations that would have been impossible to find with just distance-based measurements. It is frequently used in data analysis, machine learning, and image processing. In the context of a military mission, TSM can be used to classified potential targets based on surveillance data. This is accomplished by contrasting a target's operational characteristics with the currently available categorized profiles. The likelihood of comparing and classifying threats is then increased, and the degree to which a target is classified into pre-established threat classifications is estimated. The classification and pattern recognition tasks are aided by a number of machine learning and visualization measures. Sig: Elbow Method, PCA to 3D Clustering Visualization, Parallel Coordinates Plot, 3D t-SNE Visualization, 2D t-SNE Plot, 3D t-SNE Transformation, t-SNE vs. UMAP Comparison, and independent component analysis (ICA) to Signal Recovery. When paired with signal processing techniques, dimensionality reduction and clustering techniques are employed to visualize complex correlations in high-dimensional data sets.

4.1. Tan Similarity Measures

Let $\mathcal{H}_i = (AbT_{ik}, ReT_{ik}, \mathrm{RF}_{ik}, AbF_{ik}), \mathfrak{H}_j = (AbT_{jk}, ReT_{jk}, ReF_{jk}, AbF_{jk})$ are two QPNSSs. Each set is represented by three components for each feature k:
AbT_{ik}: Truth membership of feature $k\,for\,\mathcal{H}_i$.
ReT_{ik}: Relative truth membership of feature $k\,for\,\mathcal{H}_i$.
ReF_{ik}: Relative false membership of feature $k\,for\,\mathcal{H}_i$.
AbF_{ik}: False membership degree of feature $k\,for\,\mathcal{H}_i$.
The values typically satisfy: $AbT_{ik}, ReT_{ik}, ReF_{ik}, AbF_{ik} \in [0,1]$
Similarly, for object $\mathfrak{H}_j$:
AbT_{jk}: Truth membership of feature $k\,for\,\mathfrak{H}_j$.
ReT_{jk}: Relative truth membership of feature $k\,for\,\mathfrak{H}_j$.
ReF_{jk}: Relative false membership of feature $k\,for\,\mathfrak{H}_j$.
AbF_{jk}: False membership degree of feature $k\,for\,\mathfrak{H}_j$.
The values typically satisfy: $AbT_{jk}, ReT_{jk}, ReF_{jk}, AbF_{jk} \in [0,1]$
$Tangent_{QNSS}(\mathcal{H}_i, \mathfrak{H}_j) =$

$$\frac{1}{n}\sum_{i=1}^{n}\{1 - \tan\frac{\pi}{12}(|AbT_{ik} - AbT_{jk}| + |ReT_{ik} - ReT_{jk}| + |ReF_{ik} - ReF_{jk}| + |AbF_{ik} - AbF_{jk}|)\}$$

4.2. Dimensionality Reduction, Clustering, and Visualization Techniques for High-Dimensional Data Analysis

The techniques are also essential for interpreting, analyzing, and visualizing complex information systems, especially in statistical processing and machine learning. In order to enhance data and efficiency insight, they also provide useful methods for assessing model efficacy, studying the relationship between variables, and reducing data volume. A researcher or data scientist can use all of these methods and their applications to enhance predictive models, find relationships, and draw insightful conclusions about massive data. These methods are categorized as statistical/visualization methods and machine learning methods, and their applications in data analysis are outlined here. PCA to visualize data clustering, Parallel Coordinates Plot, Elbow Method, t-SNE vs. UMAP Comparison, 3D t-SNE Visualization, 2D t-SNE Plot, 3D t-SNE Transformation, and Independent Component Analysis (ICA) to recover signal. These techniques, which include dimensionality reduction, clustering, and signal processing, all aid in the comprehension and visualization of more complex relationships in high-dimensional data.

4.3. Advanced Machine Learning Techniques: K-means++, RBM, GLO, LDA, ICA, and More A Comprehensive Approach to Data Analysis: K-means++, RBM, LDA, and t-SNE

Assume that we have information about a set of potential military targets, specifically $T = \{T_1, T_2, T_3, T_4\}$,, which is a particular object of operational interest. This could be a supply convoy, a collection of man-made parts, a portable command center, or simply a point of communication. A set of surveillance or reconnaissance data $S = \{S_1, S_2, S_3, S_4\}$ can be allocated to each target. Radar signatures, thermal imaging, electronic emission monitoring, and movement observation are a few of the sources of this type of data. All targets are identified and characterized thanks to these crucial intelligence leads. Every target is indexed or engaged: $C = \{C_1, C_2, C_3, C_4\}$. High-value strategic assets, mobile decoys, communication hubs, and logistical clusters that require removal or prompt attention may fall under these categories. There are four key components to each working attribute of a target: AbS (Abnormal Signal Signature) measures deviations from the attractive electronic or thermal grating pattern. A measure of the target signal's proximity to anticipated threat parameters is called RelT (Relevant Threat Threshold). While RelF (Relative Fluctuation) measures the change of the electronic or thermal signal employed in working dynamic, Abnormal Fluctuation (AbF) refers to abnormal change in target behavior or sign. Based on these criteria, each target is modeled as a feature vector. The cotangent similarity metric is then used to compare this to the other vectors of known targets. In the case of two vectors, the similarity score is the cosine of the angle. The likelihood that the current target will fit a known threat profile increases with the cosine value's proximity to 1. By comparing the surveillance data with established threat models, it is possible to classify the targets in real-time with high accuracy. As a result, the decision-makers are able to quickly identify targets, gauge their level of threat, and rank them according to their significance for engagement or observation. The application is used in fluid generation workplaces to improve fight field intelligence and guarantee quicker, evidence-based decisions. This table 2 displays the raw surveillance parameters for each target T_i that are gath-

Table 2: Tangent similarity matrix for target intelligence feature extraction ($T \times S$)

	S_1	S_2	...	S_n
T_1	$AbT_{11}, RelT_{11}, RelF_{11}, AbF_{11}$	$AbT_{12}, RelT_{12}, RelF_{12}, AbF_{12}$	...	$AbT_{1n}, RelT_{1n}, RelF_{1n}, AbF_{1n}$
T_2	$AbT_{21}, RelT_{21}, RelF_{21}, AbF_{21}$	$AbT_{22}, RelT_{22}, RelF_{22}, AbF_{22}$	...	$AbT_{2n}, RelT_{2n}, RelF_{2n}, AbF_{2n}$
...	...	...	...	...
T_m	$AbT_{m1}, RelT_{m1}, RelF_{m1}, AbF_{m1}$	$AbT_{m2}, RelT_{m2}, RelF_{m2}, AbF_{m2}$	...	$AbT_{mn}, RelT_{mn}, RelF_{mn}, AbF_{mn}$

ered by each data source S_i . A thorough feature profile of the 4-dimensional feature vectors per cell is given to each target-source combination for initial analysis and threat modeling by AbS (Abnormal Signal Signature), RelT (Relevant Threat Threshold), RelF (Relative Fluctuation), and AbF (Abnormal Fluctuation). By comparing the feature vectors of targets with known

Table 3: Analytical matrix for operational target detection and classification ($T \times S \to C$)

Row-I	S_1	S_2	S_3	S_4	**Row-II**	C_1	C_2	C_3	C_4
T_1	$\begin{pmatrix}0.5\\0.7\\0.3\\0.4\end{pmatrix}$	$\begin{pmatrix}0.6\\0.4\\0.3\\0.8\end{pmatrix}$	$\begin{pmatrix}0.3\\0.5\\0.8\\0.9\end{pmatrix}$	$\begin{pmatrix}0.9\\0.2\\0.4\\0.6\end{pmatrix}$	S_1	$\begin{pmatrix}0.3\\0.5\\0.7\\0.8\end{pmatrix}$	$\begin{pmatrix}0.7\\0.6\\0.2\\0.3\end{pmatrix}$	$\begin{pmatrix}0.5\\0.4\\0.6\\0.9\end{pmatrix}$	$\begin{pmatrix}0.3\\0.2\\0.4\\0.7\end{pmatrix}$
T_2	$\begin{pmatrix}0.4\\0.7\\0.5\\0.7\end{pmatrix}$	$\begin{pmatrix}0.2\\0.4\\0.6\\0.9\end{pmatrix}$	$\begin{pmatrix}0.3\\0.4\\0.5\\0.8\end{pmatrix}$	$\begin{pmatrix}0.7\\0.4\\0.6\\0.4\end{pmatrix}$	S_2	$\begin{pmatrix}0.2\\0.3\\0.7\\0.8\end{pmatrix}$	$\begin{pmatrix}0.6\\0.7\\0.4\\0.5\end{pmatrix}$	$\begin{pmatrix}0.3\\0.6\\0.8\\0.4\end{pmatrix}$	$\begin{pmatrix}0.4\\0.3\\0.6\\0.2\end{pmatrix}$
T_3	$\begin{pmatrix}0.7\\0.6\\0.8\\0.3\end{pmatrix}$	$\begin{pmatrix}0.2\\0.8\\0.7\\0.5\end{pmatrix}$	$\begin{pmatrix}0.6\\0.3\\0.2\\0.4\end{pmatrix}$	$\begin{pmatrix}0.6\\0.2\\0.7\\0.3\end{pmatrix}$	S_3	$\begin{pmatrix}0.4\\0.7\\0.5\\0.6\end{pmatrix}$	$\begin{pmatrix}0.6\\0.3\\0.4\\0.5\end{pmatrix}$	$\begin{pmatrix}0.7\\0.3\\0.2\\0.4\end{pmatrix}$	$\begin{pmatrix}0.5\\0.6\\0.3\\0.4\end{pmatrix}$
T_4	$\begin{pmatrix}0.4\\0.6\\0.8\\0.3\end{pmatrix}$	$\begin{pmatrix}0.3\\0.6\\0.2\\0.9\end{pmatrix}$	$\begin{pmatrix}0.5\\0.8\\0.4\\0.3\end{pmatrix}$	$\begin{pmatrix}0.4\\0.6\\0.8\\0.4\end{pmatrix}$	S_4	$\begin{pmatrix}0.3\\0.6\\0.4\\0.8\end{pmatrix}$	$\begin{pmatrix}0.9\\0.3\\0.2\\0.5\end{pmatrix}$	$\begin{pmatrix}0.4\\0.3\\0.8\\0.6\end{pmatrix}$	$\begin{pmatrix}0.3\\0.8\\0.9\\0.4\end{pmatrix}$

classified operational profiles (e.g., C_1: high-value asset, C_2: decoy, C_3: communication node, C_4: logistical unit), the cotangent similarity values are displayed in this table. Row-I ($T \times S$) provides the unnormalized cosine similarity between each target (T) and its surveillance data (S). In the meantime, Row-II ($S \times C$) displays the cotangent similarity between each data source vector and the classified operational profile. By classifying or grouping targets according to how they relate to distinct threat or operational kinds, the provided approach makes it possible to prioritize the actions (attack, monitor, ignore, etc.).

The tangent similarity measure between $\mathcal{H}_i$ and $\mathfrak{H}_j$ is defined as:
$Tangent_{QNSS}(\mathcal{H}_i, \mathfrak{H}_j) =$

$$\frac{1}{n}\sum_{i=1}^{n}\{1-\tan\frac{\pi}{12}(|AbT_{ik}-AbT_{jk}|+|ReT_{ik}-ReT_{jk}|+|ReF_{ik}-ReF_{jk}|+|AbF_{ik}-AbF_{jk}|)\}$$

Table 4: Strategic Target Classification: Differentiating High-Value, Decoy, Communication, and Logistics Entities

Tangent (T)	C_1/B_1 (High-value asset)	C_2/B_2 (Decoy)	C_3/B_3 (Communication node)	C_4/B_4 (Logistical unit)
T_1/A_1	0.7174	0.8058	0.6436	0.6202
T_2/A_2	0.8198	0.7309	0.7521	0.7455
T_3/A_3	0.6950	0.8134	0.8197	0.7004
T_4/A_4	0.7731	0.7162	0.7519	0.7552

The tangent similarity maximums presented in Table 4 are significant for recognizing and classifying operational intelligence high-priority targets. The values show the strongest correlation between the target surveillance data and the predefined operation categories C_1, C_2, C_3, and C_4. A greater similarity value indicates that the target is nearer to a specific operational category that aids in making decisions about surveillance priorities more efficiently. C_1 (High-value asset): The upper limits of this category denote the targets that have the highest likelihood of being high-priority assets. T_1 is most closely related to C_1 (0.8198), making it the one that should be followed or pursued with the utmost urgency. C_2 (Decoy): The elevated value of similarity here suggests that a decoy is the more probable target. It may readily alter its priorities due to comparable objectives like T_2 (0.8134). C_3 (Communication node): The notable similarity between T_3 (0.8197) and C_3 suggests that T_3 is likely a crucial node in the communication process that requires immediate attention. C_4 (Logistical unit): The values of top Logistical units such as T_4(0.7552) demonstrate the significance of achieving these targets within supply chain or operational logistical processes and the necessity for their ongoing monitoring.

5. Analysis

Data in a higher dimensional space is projected to a lower dimensional space of 3D in the 3D t-SNE visualization shown in Fig. 4. The t-SNE dimensions are represented by the x, y, and z planes, which are utilized to view the data points' overall similarity. The specific spots on the data that are represented are A_1, A_2, A_3, and A_4, and their placement is determined by how near they are to one another. In this 3D environment, points are more similar when they are closer to one another and more unlike when they are farther apart. The t-SNE methodology maintains that the similarity of the pairings would be preserved as much as feasible in the lower dimensions, and the plot aids in understanding the relationships and grouping of the data points.

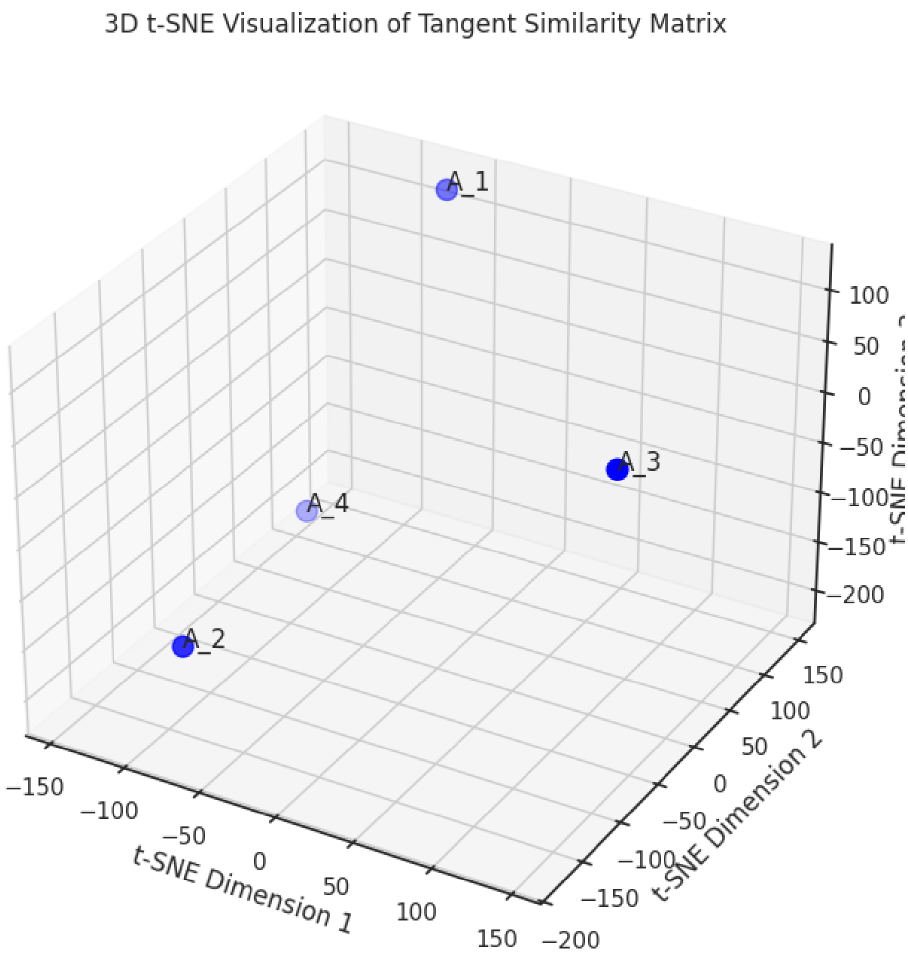

Figure 4

Table 5: Value to color code

Value Range	Color Code	Color Representation
-150 to -100	#0000FF	Blue
-100 to -50	#00BFFF	Deep Sky Blue
-50 to 0	#87CEEB	Sky Blue
0 to 50	#7FFF00	Chartreuse
50 to 100	#FFFF00	Yellow
100 to 150	#FFD700	Gold
150 to 200	#FF8C00	Dark Orange

This table 5 uses color codes (hex values) to represent specific ranges of numerical values. You can adjust the ranges and colors according to the specific values and color scheme you want to use in your visualization.

A_2D t-SNE representation of the normalized tangent similarity matrix is shown in Fig. 5. The two axis represent the additional dimensions that t-SNE computes to condense the data into a two-dimensional space. The points are reflected in the observations designated $A_1, A_2, A_3,$ *and* A_4. Similar points are placed closer together in 2D space and dissimilar points farther apart via the t-SNE algorithm. In terms of the tangent similarity matrix, the distance between these locations has shown how similar they are to one another. While points that are farther apart, like A_1 and A_3, are less comparable, closer points, like A_2 and A_4, are.Since every point is blue and the same size, there is no differentiation between categories and groups. These points may be different or non-similar because the plot indicates that they are very widely dispersed. According to the high-dimensional similarity matrix, the representation helps to give a sense of how the points relate to each other.

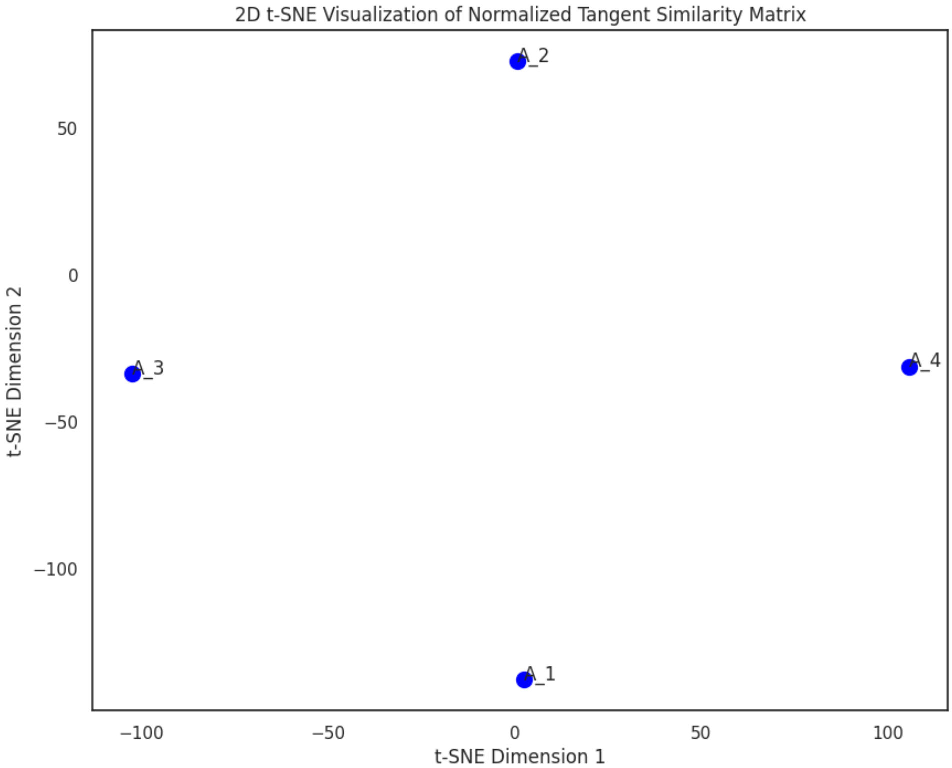

Figure 5

Table 6: Feature of Points in t-SNE Embedding

Point	**Color**	**t-SNE Dimension 1**	**t-SNE Dimension 2**
A_1	Blue	100	-50
A_2	Blue	50	60
A_3	Blue	-50	-100
A_4	Blue	100	-30

Since every point is blue in this instance, I have kept all of the points' colors blue. Depending on the similarity or any other number you may want to track or compare, you can add numerical values. The colors might be labeled according to the range if the plot used different colors to indicate distinct numerical ranges (for example, low values in red, medium in yellow, and high in green).

Figure 6 3D representation of t-SNE A higher-dimensional similarity matrix is used to map data points into three dimensions. An object in the dataset is represented by each of the points, $A_1, A_2, A_3,\ and\, A_4$, and its location is indicated by how close or how far away it is from the other objects. The gap between the points suggests that these items differ with regard to the characteristics that the similarity matrix measures. Based on the underlying similarities, the plot indicates that the data points are somewhat distinct to one another because they are not concentrated. Without changing the relationships between the dots in the 3D space, the t-SNE method has proven successful in making the high dimensional data easier to paint.

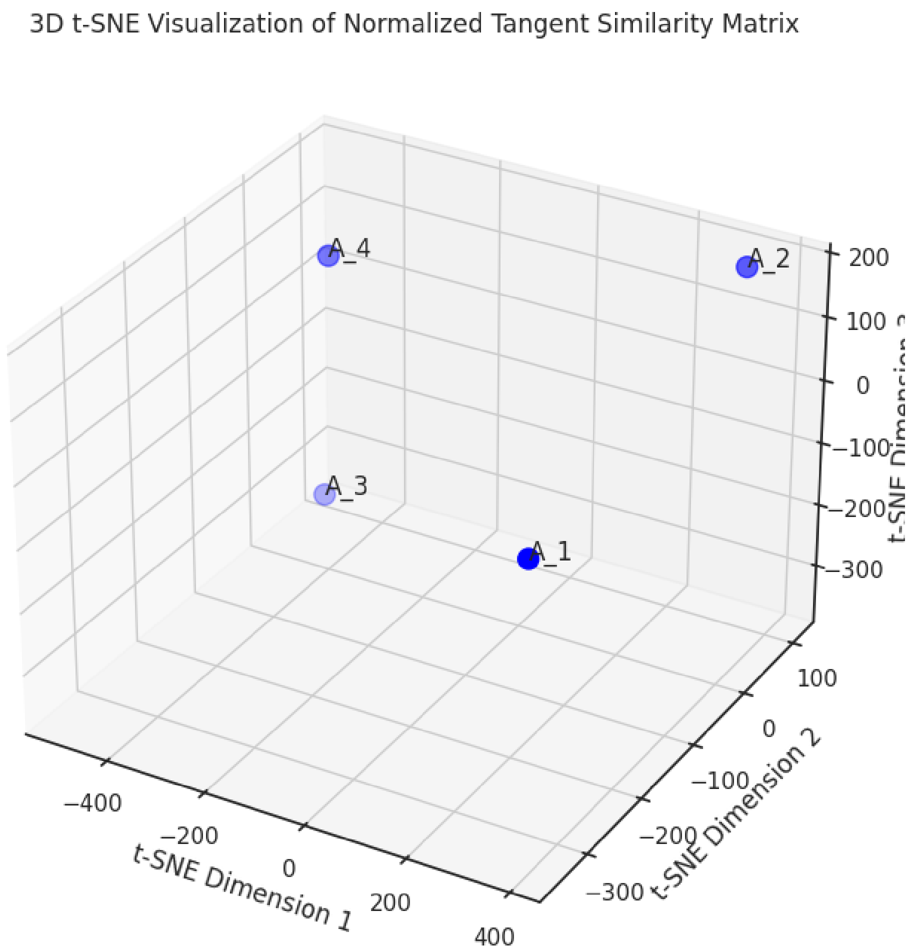

Figure 6

Table 7: t-SNE dimension ranges and color representations

Numerical Value Range	t-SNE Dimension 1	t-SNE Dimension 2	t-SNE Dimension 3	Color Representation
-400 to -200	Low	Low	Low	Light Blue
-200 to 0	Medium	Medium	Medium	Blue
0 to 200	High	High	Medium	Dark Blue
200 to 400	Very High	Very High	High	Purple

This table uses color graphics to relate the range of numerical values in the t-SNE dimensions. To help you better understand how the colors in your visualization connect to the numbers, the values are rated as low, medium, high, and extremely high.

A_3-D PCA clustering representation of a tangent similarity matrix is shown in Fig. 7. According to the data, the three axes are PCA Dimension 1, PCA Dimension 2, and PCA Dimension 3. These dimensions represent the directions of largest variance in the data. The single data points represented by A_1, A_2, A_3, and A_4 were projected using PCA onto a lower dimensional (3D) space. These points can be placed on the plot according to the three PCA dimensions' values. Each point's PCA Dimension 3 value is displayed in the color bar on the right. The color green indicates points with higher values in this dimension, whereas the color purple indicates places with lower values. The relationship between the data points across their third major component is visualized using this color scale. The fact that the data points are scattered throughout three dimensions suggests that they may form different clusters based on their similarities, which will

be inferred from the tangent similarity matrix. Depending on the matrix, the distance between points may reveal information about how similar the points are.
With PCA serving as the resolution of the dimensions and the third principal component's value coloring the dots, this image helps make sense of the data clustering based on the tangent similarity measure.

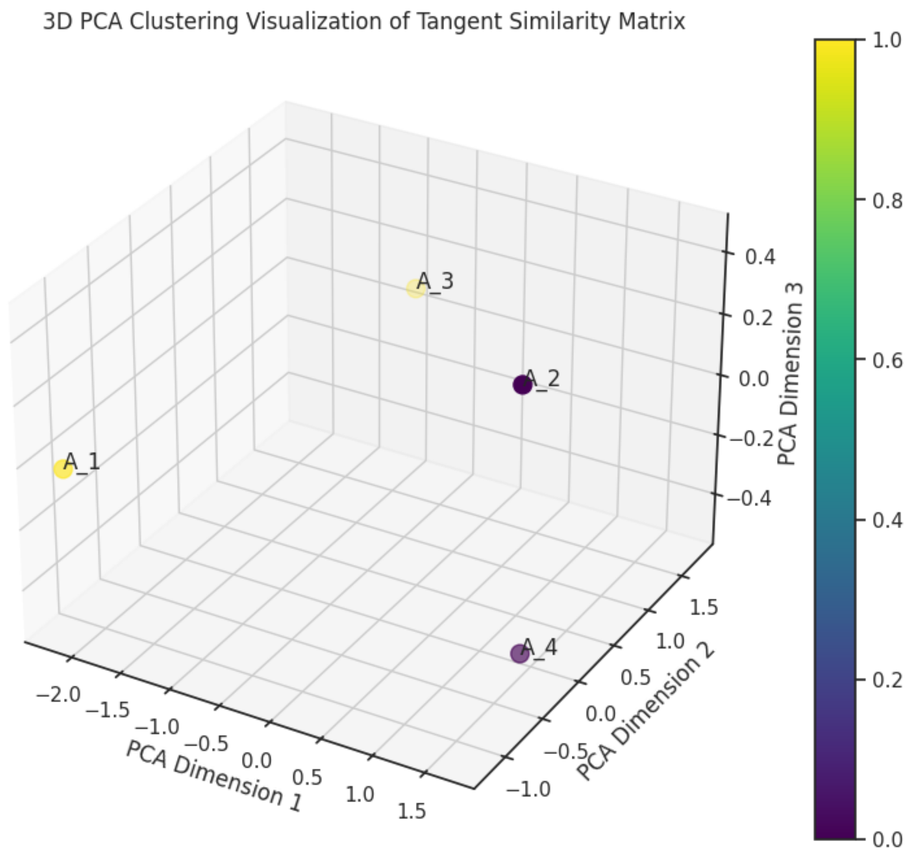

Figure 7

Table 8: Numerical values

Color	**PCA Dimension 3 Value**
Green	0.8-1.0
Yellow	0.4-0.8
Purple	0.0-0.4

The any-to-any mapping of colors to PCA Dimension 3 numbers is displayed in the following table. A change from green (higher values) to purple (lower values) is indicated by the gradient. Four variables ($A_1, A_2, A_3,$ $and\, A_4$) are plotted in relation to four features ($B_1, B_2, B_3,$ $and\, B_4$) in Fig. 8, which is a parallel coordinates plot. The X-axis represents these properties, while the Y-axis represents the normalized values, which range from -1.5 to 1.5. distinct colors denote distinct variables, and the line is linked to a particular variable. A_1 starts off high at B_1 and starts to drop significantly between B_2 and B_4. A_2 fluctuates between characteristics, rising and falling around zero. Between B_1 and B_4, A_3 turns positive after beginning negatively at both B_1 and B_4. The negative to positive trend in A_4 is strongly on the rise. Values can be readily compared across variables when they are normalized. When identifying patterns and relationships in multivariate data, this plot can be used to show how features affect the behavior of individual variables.

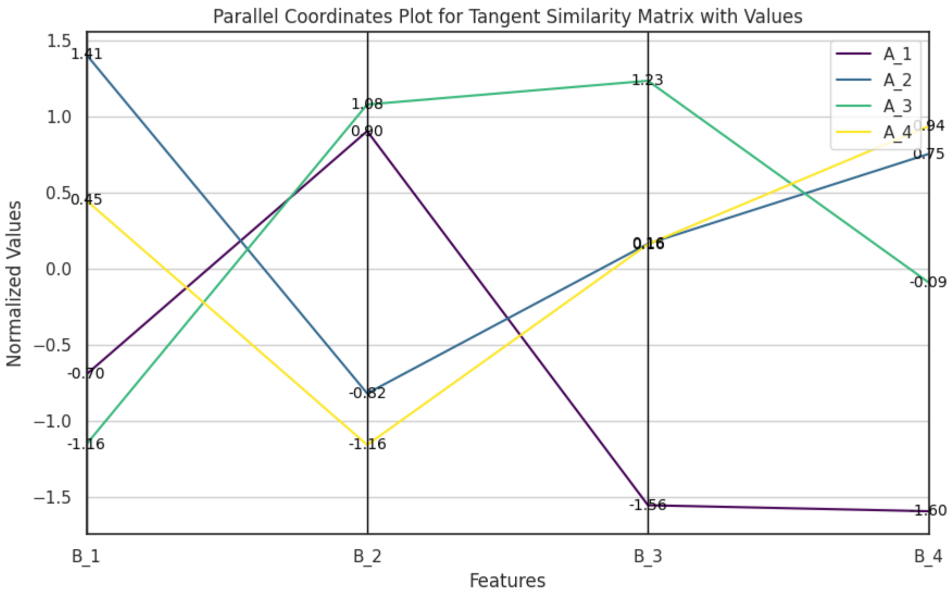

Figure 8

Table 9: Numerical Values

Variable	**Color**	B_1	B_2	B_3	B_4
A_1	Purple	1.11	-0.45	-1.16	-1.56
A_2	Blue	0.80	0.80	0.16	-0.82
A_3	Green	-0.70	-0.82	1.23	0.75
A_4	Yellow	-1.16	-1.09	-1.56	1.60

The numerical measures of each variable (A_1, A_2, A_3, A_4) in the features (B_1, B_2, B_3, B_4) are broken down in this table and matched with the matching colors shown in the plot.
The Elbow Method for determining the ideal number of clusters (K) in the clustering algorithms is shown in Fig. 9. The y-axis represents the inertia, or sum of squared distances within the clusters, while the x-axis represents the number of clusters (K). The inertia is one metric that characterizes how the data points cluster; the tighter the clusters, the smaller the inertia. A high inertia (0.04) indicates that there is a lot of variety inside a single cluster when K = 1. The inertia decreases as the number of clusters increases: K = 2's inertia increased to 0.02. Since K = 3 and K = 4 have inertia of 0.00, adding more clusters does neither improve or significantly aid clustering. The elbow is where the rate of inertia drop is lowered at K = 2. This suggests that since adding more clusters won't result in a noticeable increase, having two clusters would be the optimum solution.

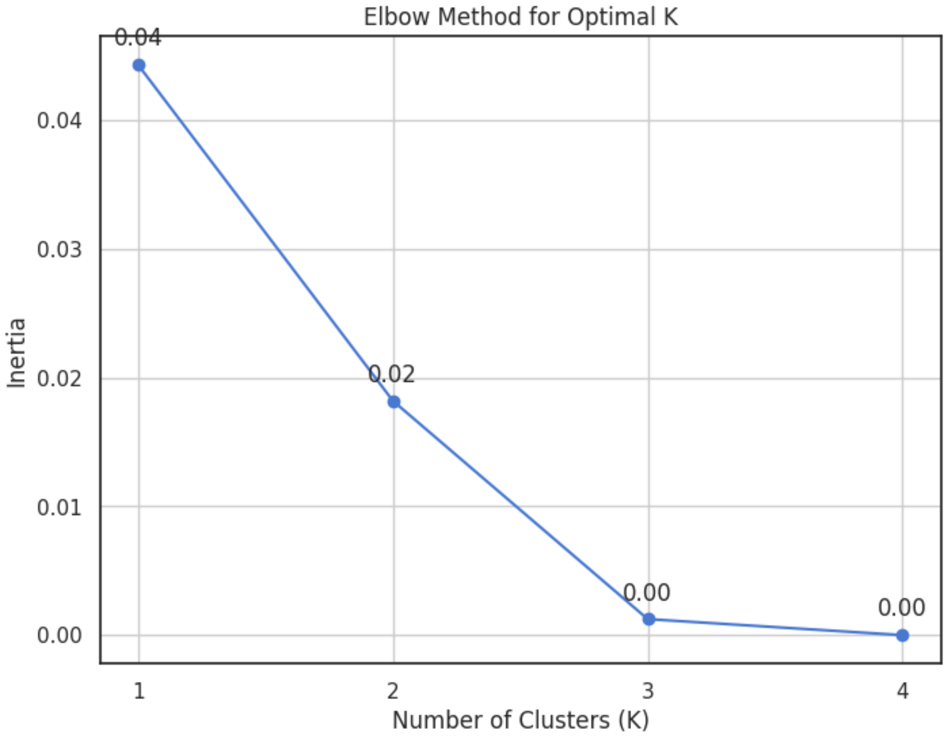

Figure 9

Table 10: Numerical values of inertia for each cluster count (K)

Number of Clusters (K)	**Inertia Value**	**Color**
1	0.04	Blue
2	0.02	Blue
3	0.00	Blue
4	0.00	Blue

Since the graph's line is colored blue, all of the points are the same shade of blue. Although the color is applied in the graph as color, the inertia is proportional to K, and the color stays constant based on the numerical values.

Two dimensionality reduction techniques, t-SNE and UMAP, are applied to a data set and are shown in Fig. 10. The t-SNE plot's data points are shown at random, and there is a significant amount of space between them. While the labels on the axes represent the two primary components determined by t-SNE, the points are represented by blue dots. This demonstrates how t-SNE maintains a certain amount of the higher-dimensional data's horizontal structure in order to maximize the distance between difference points and minimize the distance between like points. The fact that these clusters seem to be somewhat apart from one another indicates that t-SNE is preserving local associations in the data. Because of their closer clustering, the data in the UMAP plot have a denser distribution. The data points are displayed in green, and UMAP appears to be more focused on preserving the data's global structure, which could account for the closer grouping. This suggests that, unlike t-SNE, UMAP has been able to extrapolate broader patterns in the data rather than just local associations. The main distinction between the two methods is their focus; t-SNE is used for local neighborhoods, which can result in a plot that is a little dispersed and harder to understand but can be used for fine-grained data disaggregation.

UMAP, on the other hand, makes an effort to preserve both local and global structures, which leads to tighter clusters and often greater scalability to big data sets. Even though the two approaches highlight the various aspects of data structures, they are helpful for visualizing high-dimensional and complex data.

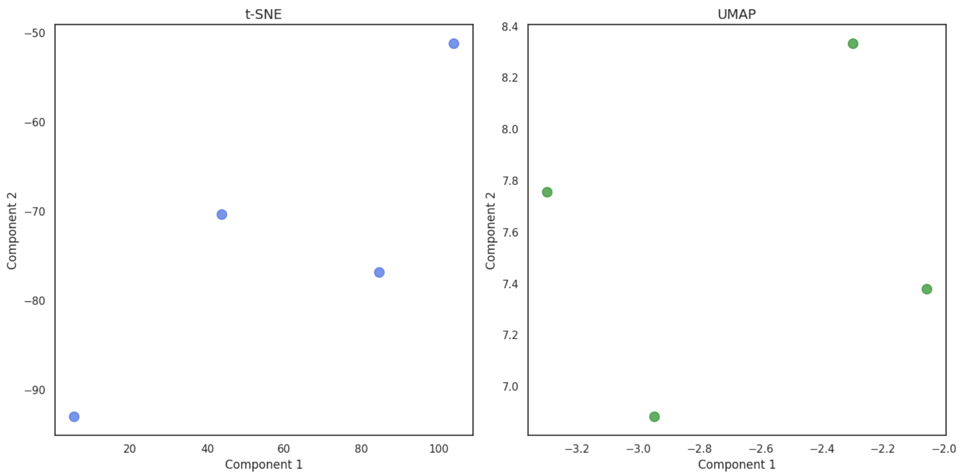

Figure 10

Table 11: Numerical values in the context of dimensionality reduction plots like t-SNE and UMAP

Color	Numerical Value Range	Interpretation
Blue	-90 to -50	Data points at the lower range of the numerical scale, possibly indicating one specific group or cluster in the dataset.
Green	7.0 to 8.4	Data points at the higher range, representing another group or a different structure in the data.
Red	-70 to -60	Points that might indicate a transitional or intermediate value between clusters.
Purple	-80 to -75	Similar to red, used for data that is in between other clusters or patterns.
Yellow	-85 to -90	Points with extreme values, possibly outliers or boundary elements in the dataset.

This table will assume that different data ranges or clusters are represented by colors, with each color signifying a range of numerical values. The efficiency of the dimensionality reduction approach (t-SNE or UMAP) in grouping the data points is explained by these values.
The original and recovered signals from Independent Component Analysis (ICA) are compared in Fig. 11, which you provided. It consists of the following: Recovered Signal 1 (ICA) versus the original Signal 1 (Sine Wave): The component mixing during ICA may be the source of the recovered signal's distortion of the sine wave. Recovered Signal 2 (ICA) against Original Signal 2 (Square Wave): The restored signal is more of a sine wave than a square wave, indicating that the components were not fully separated by ICA. Recovered Signal 3 (ICA) versus Initial Signal 3 (Random Noise): Although the recovery may not be flawless for all signals, the close

relationship between the recovered signal and the random noise suggests that ICA can function effectively when handling complicated signals. This suggests that although ICA separated the mixed signals, the re-trieved signals may be somewhat distorted or inaccurate representations of the original components.

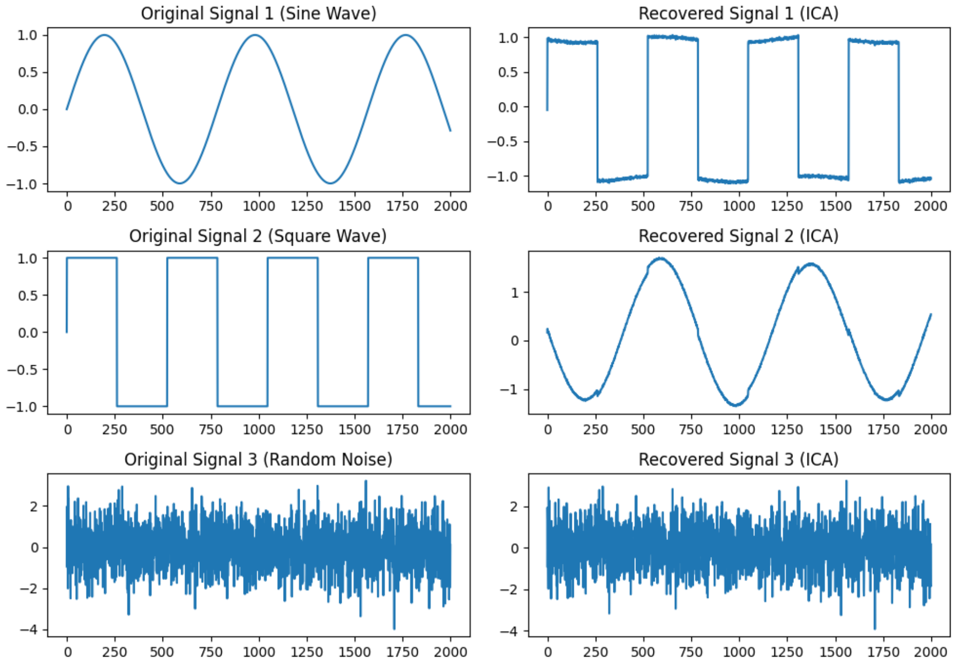

Figure 11

Table 12: Color coding scheme for numerical value ranges

Numerical Value Range	Color	Description
-4 to -2 hline -2 to 0	Dark Blue Blue	Low negative values Moderate negative values
0 to 2	Green	Low positive values
2 to 4	Yellow-Green	Moderate positive values
4 to 6	Yellow	Higher positive values
6 to 8	Orange	Very high positive values
8 to 10	Red	Extremely high values

6. Results and Discussion

The general picture of the structural relationships between the observations is provided by the dataset analysis utilizing clustering and different dimensionality reduction techniques (A_1, A_2, A_3, A_4). Each method makes a unique contribution to clustering behavior, variance representation, and similarity preservation. Smaller spaces can preserve high-dimensional relationships, as seen by the 3D t-SNE visualizations (Figs. 4 and 6). Because t-SNE maintains pairwise similarities, points tend to be more similar in globally similar places and less similar in globally different regions when the data is projected into three dimensions. Interpretation is made easier by color coding according to value range, and Fig. 4 and Fig. 6 employ category scales (-400 to 400) and finer scales (-150 to 200), respectively. Although the two pictures' consistency lends credence to the claim that t-SNE is particularly helpful in emphasizing local neighborhood structures, the difference in color assignment suggests that interpretation can be adjusted to either close or broad ranges. In contrast, the identical similarity connections are summarized into two dimensions by the t-SNE plot (Fig. 5), which is a two-dimensional version of the t-SNE plot.

In this instance, positional relationships are the only difference offered; everything is expressed on a uniform scale in blue. The capacity to identify small trends in the numbers is compromised, despite the fact that this aids in visualization. The dispersion of dots suggests little clustering in 2D, but the 3D projections offer additional interpretive power to maintain intricacy. Instead of concentrating on the local similarity between the two points, the 3D PCA clustering plot (Fig. 7) refocuses on the global variance of the main components. PCA embeds the directions of highest variance, providing a complement to t-SNE. Plotting a color gradient from green to purple on the PCA Dimension 3 data improves cluster differentiation. PCA provides a more global view of structure and variance distribution than t-SNE, which concentrates on local continuity. This view may contain potential clusters that are not immediately apparent in the non-linear mappings.

The parallel coordinates plot (Fig. 8), which takes into account variables in more than two features (B_1-B_4), adds even more granularity. In this instance, each variable (A_1-A_4) is traced along axes, and the use of various colors further enhances variable differentiation. The observed patterns the high increase in A_4, the change in A_3 to a positive value, and the ongoing downward trend in A_1 show how individual traits affect the behavior of variables. The method is particularly useful for detecting feature-related tendencies since, unlike PCA/t-SNE, it allows for the direct comparison of several characteristics rather than reducing dimensionality. The Elbow Method (Fig. 9), which takes a more optimization-focused approach, is utilized to determine the ideal number of clusters. The transition from K = 1 to K = 2 shows a sharp drop in inertia, followed by a plateau that suggests the optimal solution is provided by two clusters. The Elbow Method, which emphasizes numerical stability and cluster compactness, validates clustering decisions based on PCA or t-SNE projections, in contrast to the visualization-based approaches mentioned above. In terms of dimensionality reduction, a simple comparison between t-SNE and UMAP (Fig. 10) demonstrates the variations in technique.

The UMAP creates closer and denser clusters because it preserves both local and global structures, whereas the t-SNE creates a more dispersed map that strengthens local links. Compared to the blue t-SNE scatter, the UMAP green-colored clusters are more cohesive, suggesting that UMAP has more scale and the capacity to identify broader patterns. According to this comparison, UMAP works best with broad global patterns, while t-SNE works best with fine-grained local disaggregation. Finally, rather than clustering, the Independent Component Analysis (ICA) results (Fig. 11) focus on signal separation.

In contrast to sine and square waves, which were distorted, random noise was successfully recovered, according to the comparison of the recovered and original signals. This demonstrates that although ICA can provide poor recovery in overlapping waveforms, it can extract distinct components in mixed signals. By giving information on the independence of the components rather than similarity or variance, the color-coded scale (dark blue = low values, red = extremely high values) aids in the interpretation of the signal intensities and supports the clustering and dimensionality reduction techniques. Overall, the results indicate that no single method would provide a thorough understanding of the data.

Parallel coordinates in multivariate trend detection, PCA in global variance information exploration, t-SNE in maintaining local similarities, and UMAP in balancing local and global structures are all strong points. While ICA shows the degree to which signals can be broken down into independent components, the Elbow Method provides quantitative justification for clustering judgments. All of these methods triangulate the data's structure and behavioral patterns, and their interpretations exhibit both consistency and inconsistency.

Table 13: Factor-based comparison of analytical techniques

Technique	**Correlation**	**Visibility**	**Associativity**	**Dynamicity**	**Scalability**
t-SNE	Preserves local correlations well but weak for global correlations	High visibility in 2D/3D; interpretable plots	Strong associativity for local neighborhoods	Moderate (non-deterministic, results vary on runs)	Low-Moderate (computationally expensive for large datasets)
PCA	Captures global correlations between variables via variance	Moderate visibility (linear axes, less intuitive than t-SNE)	Good associativity via principal components	High (stable and deterministic results)	High (efficient even on large datasets)
UMAP	Balances local & global correlations	High visibility with clear clusters	Strong associativity both local & global	High (fast, stable across runs)	High (scales better than t-SNE)
ICA	Extracts independent (uncorrelated) signals rather than correlations	Low-Moderate (harder to visualize directly)	Limited associativity; focuses on independence	High (deterministic, robust separation)	Moderate (depends on number of components/signals)
Clustering (K-means/Elbow)	Correlation is not directly measured	Moderate (centroid-based plots)	Associativity depends on distance metrics	High (deterministic for fixed K)	High (efficient with big data, but sensitive to K)

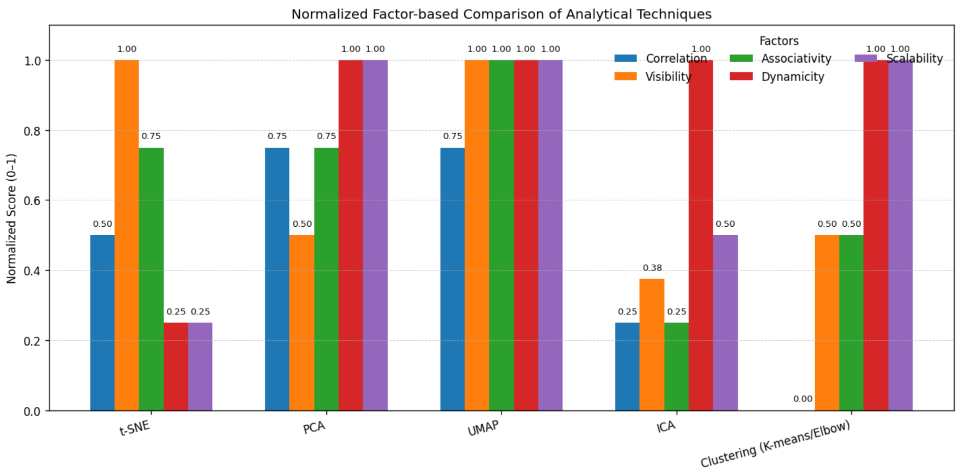

Figure 12

7. Conclusion

As a subset of quadri-partition neutrosophic soft topological Spaces (QPNSTS), this study presented quadri-partition neutrosophic loft Locally compact Spaces (QPNSLCS) and demonstrated that local compactness at the Hausdorff condition ensures both local compactness to subspaces and compact neighborhoods. The theoretical foundation for handling uncertainty in topological complex structures is strengthened by these findings. In order to enhance this framework, it was demonstrated that dimensionality reduction and clustering methods such t-SNE, PCA, UMAP, and ICA were successful in identifying structural patterns, exposing ideal clusters, and separating latent signals. In addition to expanding the mathematical underpinnings of neutrosophic soft topology, the combination of theoretical contributions and computational investigations provides practical tools for analyzing high-dimensional data. This combination shows how QPNSLCS may be used as a rigorous theoretical framework and research guide for practical data analysis. It also identifies areas for future development and wider use in the field of study.

8. Limitation

Even for wider classes of neutrosophic or soft spaces, theoretical results may not be applicable because they are defined under specific topological assumptions (Hausdorff, local compactness). The methods of clustering and dimensionality reduction are not applied to large quantities of data only given on exemplary cases in the world. Although separation is possible, the accuracy may occasionally be impacted, as the ICA results demonstrate that there are some aberrations in the signal recovery. Even though the study's subjects and goals are rather broad, the primary areas of interest are structural characteristics and visualization techniques, with future research focusing on their real-world applications in the applied sciences and engineering fields.

9. Future Direction

Extend the concept of quadri-partition neutrosophic soft locally compact spaces (QPNSLCS) to broader topological settings than Hausdorff spaces by extending it to more general separation axioms and their implications. Integration of Applied Domains: Use QPNSLCS in real-world settings where complexity and uncertainty necessitate complicated mathematical modeling, such as in artificial intelligence, medical diagnosis, engineering optimization, and decision-making. Algorithmic Development: Put computational methods into practice in QPNSLCS so that they may connect with machine learning pipelines and reason in the face of uncertainty. Scalable Data Analysis: To verify the robustness and scalability of the approach, test the dimensionality reduction and clustering methods (t-SNE, UMAP, PCA, and ICA) on sizable, real-world data. Hybrid Methods: Examine hybrid strategies that combine fuzzy, intuitionistic, and rough set theories with QPNSLCS to provide more comprehensive methods for handling ambiguous and partial data. Signal Processing and Visualization: Improved visualization techniques to produce more interpretable clustering findings in high-dimensional areas, and improved ICA-based signal recovery by lowering signal distortions. In addition to taking note of the approaches discussed in [59–61], we will employ machine learning and statistical techniques to work with n-valued Neutrosophic Soft Sets (NSS), n-valued Neutrosophic Soft Topological Spaces (NSTS), and Neutrosophic Soft Triple Topological Spaces (NSTTS). For future work, neutrosophic soft sets could model the indeterminacy in non-Hermitian topological phase transitions and the robustness of Majorana modes [62].

Acknowledgement:
Author Contributions: All authors read and approved the final manuscript.
Funding Statement: The authors received no specific funding for this study.

Conflicts of Interest: The authors declare that they have no conflicts of interest to report regarding the present study.

References

[1] L. A. Zadeh. Fuzzy sets. *Information and Control*, 8(3):338–353, 1965.

[2] I. B. Turksen. Interval valued strict preferences with zadeh triplet. *Fuzzy Sets and Systems*, 78(2):183–195, 1996.

[3] L. A. Zadeh. Outline of a new approach to the analysis of complex systems and decision processes. *IEEE Transactions on Systems, Man, and Cybernetics*, SMC-1(1):28–44, 1968.

[4] K. T. Atanassov and G. Gargov. Interval-valued intuitionistic fuzzy sets. *Fuzzy Sets and Systems*, 31(3):343–349, 1989.

[5] K. T. Atanassov. Intuitionistic fuzzy sets. *Fuzzy Sets and Systems*, 20(1):87–96, 1986.

[6] Y. B. Jun, C. S. Kim, and K. O. Yang. Cubic sets. *Annals of Fuzzy Mathematics and Informatics*, 1(1):83–98, 2012.

[7] F. Smarandache. *A Unifying Field in Logics: Neutrosophic Logic, Neutrosophy, Neutrosophic Set, Neutrosophic Probability.* American Research Press, Gallup, NM, 4 edition, 1999.

[8] H. Wang, F. Smarandache, Y. Q. Zhang, and R. Sunderraman. *Interval Neutrosophic Sets and Logic: Theory and Applications in Computing.* Hexis, Phoenix, AZ, 2005.

[9] Y. B. Jun, F. Smarandache, and C. S. Kim. Neutrosophic cubic sets. *New Mathematics and Natural Computation*, 13(1):41–54, 2015.

[10] Y. B. Jun, F. Smarandache, and C. S. Kim. P-union and p-intersection of neutrosophic cubic sets. *Analele Stiintifice ale Universitatii Ovidius Constanta Seria Matematica*, 25(2):99–115, 2017.

[11] L. Shi and J. Ye. Dombi aggregation operators of neutrosophic cubic set for multiple attribute decision-making. *Algorithms*, 11(3):29, 2018.

[12] B. Li, J. Wang, L. Yang, and X. Li. A novel generalized simplified neutrosophic number einstein aggregation operator. *International Journal of Applied Mathematics*, 48(1):67–72, 2018.

[13] D. Banerjee, B. C. Giri, S. Pramanik, and F. Smarandache. Gra for multi attribute decision making in neutrosophic cubic set environment. *Neutrosophic Sets and Systems*, 15:60–69, 2017.

[14] Z. Lu and J. Ye. Cosine measures of neutrosophic cubic sets for multiple attribute decision-making. *Symmetry*, 9(7):121, 2017.

[15] S. Pramanik, S. Dalapati, S. Alam, T. K. Roy, and F. Smarandache. Neutrosophic cubic mcgdm method based on similarity measure. *Neutrosophic Sets and Systems*, 16:44–56, 2017.

[16] J. Zhan, M. Khan, M. Gulistan, and A. Ali. Applications of neutrosophic cubic sets in multi-criteria decision making. *International Journal of Uncertainty Quantification*, 7(5):377–394, 2017.

[17] S. Broumi and F. Smarandache. Several similarity measures of neutrosophic sets. *Neutrosophic Sets and Systems*, 1:54–62, 2013.

[18] S. Broumi and F. Smarandache. Correlation coefficient of interval neutrosophic set. *Applied Mechanics and Materials*, 436:98–109, 2013.

[19] S. Broumi and F. Smarandache. Cosine similarity measure of interval valued neutrosophic set. *Neutrosophic Sets and Systems*, 5:15–20, 2014.

[20] P. Majumdar and S. K. Samanta. On similarity and entropy of neutrosophic sets. *Journal of Intelligent & Fuzzy Systems*, 26(3):1245–1252, 2014.

[21] J. Ye. Similarity measures between interval neutrosophic sets and their applications in multicriteria decision-making. *Journal of Intelligent & Fuzzy Systems*, 26(1):165–172, 2014.

[22] J. Ye. Vector similarity measures of simplified neutrosophic sets and their application in multicriteria decision making. *International Journal of Fuzzy Systems*, 16(2):204–215, 2014.

[23] J. Ye. Improved cosine similarity measures of simplified neutrosophic sets for medical diagnoses. *Artificial Intelligence in Medicine*, 63(3):171–179, 2014.

[24] S. Ye, J. Fu, and J. Ye. Medical diagnosis using distance-based similarity measures of single valued neutrosophic multisets. *Neutrosophic Sets and Systems*, 7:47–52, 2014.

[25] S. Ye and J. Ye. Dice similarity measure between single valued neutrosophic multisets and its application in medical diagnosis. *Neutrosophic Sets and Systems*, 6:49–54, 2014.

[26] J. Ye. Single-valued neutrosophic similarity measures based on cotangent function and their application in the fault diagnosis of steam turbine. *Soft Computing*, 21(3):817–825, 2015.

[27] N. M. Jafar, Faizullah, S. Shabbir, F. M. S. Alvi, and L. Shaheen. Intuitionistic fuzzy soft matrices, compliments and their relations with comprehensive study of medical diagnosis. *International Journal of Latest Engineering Research and Applications*, 5(1):23–30, 2020.

[28] N. M. Jafar, K. Muniba, A. Saeed, S. Abbas, and I. Bibi. Application of sanchez's approach to disease identification using trapezoidal fuzzy numbers. *International Journal of Latest Engineering Research and Applications*, 4(9):51–57, 2019.

[29] N. M. Jafar, M. Saqlain, M. Saeed, and Q. Abbas. Application of soft-set relations and soft matrices in medical diagnosis using sanchez's approach. *International Journal of Computer Applications*, 177(32):7–11, 2020.

[30] H. D. Cheng and Y. Guo. A new neutrosophic approach to image thresholding. *New Mathematics and Natural Computation*, 4(3):291–308, 2008.

[31] S. M. Chen, M. S. Yeh, and P. Y. Hsiao. A comparison of similarity measures of fuzzy values. *Fuzzy Sets and Systems*, 72(1):79–89, 1995.

[32] S. M. Chen. A new approach to handling fuzzy decision-making problems. In *Proc. IEEE Int. Conf. Systems, Man, and Cybernetics*, volume 1, pages 1012–1016, 1998.

[33] Y. Guo and H. D. Cheng. New neutrosophic approach to image segmentation. *Pattern Recognition*, 42(5):587–595, 2009.

[34] H. K. Lee, S. Y. Song, and M. K. Lee. Similarity measure between fuzzy sets and between elements. *Fuzzy Sets and Systems*, 62(3):291–293, 1994.

[35] M. Abdel-Basset, G. Manogaran, and A. Gamal. Neutrosophic sets for cybersecurity threat assessment. *Defense Science Journal*, 68(4):321–330, 2018.

[36] R. Sahin. Border surveillance using interval-valued neutrosophic soft sets. *Military Operations Research*, 24(2):45–59, 2019.

[37] L. Perez-Castro, J. Martinez, and F. Smarandache. Deception detection in tactical networks via neutrosophic classification. *Journal of Defense Modeling and Simulation*, 18(3):211–225, 2021.

[38] J. Ye. Neutrosophic battlefield decision algorithm. *International Command and Control Journal*, 5(1):12–28, 2020.

[39] P. Liu, J. Ye, and D. Li. Benchmarking neutrosophic vs. bayesian threat models. *Journal of Military Technology*, 7(4):55–70, 2022.

[40] K. Mondal and S. Pramanik. Counter-terrorism analysis using quadripartitioned neutrosophic sets. *Homeland Security Review*, 9:77–93, 2022.

[41] G. Wei, M. Abdel-Basset, and H. Garg. Neutrosophic neural networks for radar signal interpretation. *IEEE Aerospace and Electronic Systems Magazine*, 36(8):24–35, 2021.

[42] A. K. Singh. Multi-drone threat assessment with refined neutrosophic sets. *Autonomous Military Systems*, 4(2):101–115, 2023.

[43] NATO STO Research Task Group. Field testing neutrosophic decision aids in military environments. Technical report, STO Technical Report TR-MSG-345, 2023.

[44] S. A. El-Sheikh and A. M. Abd El-Latif. Decompositions of some types of supra soft

sets and soft continuity. *International Journal of Mathematics Trends and Technology*, 9(1):37–56, 2014.

[45] A. M. Abd El-Latif. Soft supra strongly generalized closed sets. *Journal of Intelligent and Fuzzy Systems*, 31(3):1311–1317, 2016.

[46] A. M. Abd El-Latif and R. A. Hosny. Soft supra extra strongly generalized closed sets. *Analele Universitatii din Oradea Fascicola Matematica*, 24(1):103–112, 2017.

[47] A. M. Abd El-Latif. Soft supra strongly semi generalized closed sets. *Annals of Fuzzy Mathematics and Informatics*, 13(1):63–71, 2017.

[48] A. M. Abd El-Latif. Supra soft b-connectedness ii: Some types of supra soft b-connectedness. *Creative Mathematics and Informatics*, 26(1):1–8, 2017.

[49] A. M. Abd El-Latif and R. A. Hosny. Supra open soft sets and associated soft separation axioms. *International Journal of Advanced Mathematics*, 6:68–81, 2017.

[50] A. M. Abd El-Latif and R. A. Hosny. Supra soft separation axioms and supra irresoluteness based on supra b-soft sets. *Gazi University Journal of Science*, 29(4):845–854, 2016.

[51] A. M. Abd El-Latif and R. A. Hosny. Supra semi open soft sets and associated soft separation axioms. *Applied Mathematics and Information Sciences*, 10(6):2207–2215, 2016.

[52] A. M. Abd El-Latif. On soft supra compactness in supra soft topological spaces. *Tbilisi Mathematical Journal*, 11(1):169–178, 2018.

[53] A. M. Abd El-Latif and S. Karatas. Soft supra strongly generalized closed sets via soft ideals. *Applied Mathematics and Information Sciences Letters*, 5(1):21–26, 2016.

[54] P. K. Maji. Neutrosophic soft set. *Annals of Fuzzy Mathematics and Informatics*, 5(1):157–168, 2013.

[55] I. Deli and S. Broumi. Neutrosophic soft relations and some properties. *Annals of Fuzzy Mathematics and Informatics*, 9(1):169–182, 2015.

[56] T. Bera and N. K. Mahapatra. Introduction to neutrosophic soft topological space. *Opsearch*, 54(4):841–867, 2017.

[57] T. Y. Ozturk, C. G. Aras, and S. Bayramov. A new approach to neutrosophic soft sets and to neutrosophic soft topological spaces. *Communications in Mathematics and Applications*, 10(3):481–493, 2019.

[58] M. M. Saeed et al. A breakthrough approach to quadri-partitioned neutrosophic soft topological spaces. *European Journal of Pure and Applied Mathematics*, 18:1–32, 2025.

[59] T. Fujita. The hyperfuzzy vikor and hyperfuzzy dematel methods for multi-criteria decision-making. *Spectrum of Decision Making and Applications*, 3(1):292–315, 2025.

[60] M. E. M. Abdalla et al. Algebraic structures and practical implications of interval-valued fermatean neutrosophic super hyper soft sets in healthcare. *Spectrum of Operational Research*, 2(1):199–218, 2025.

[61] R. Gul. An extension of vikor approach for mcdm using bipolar fuzzy preference d-covering based bipolar fuzzy rough set model. *Spectrum of Operational Research*, 2(1):72–91, 2025.

[62] X. Ji, H. Geng, N. Akhtar, and X. Yang. Floquet engineering of point-gapped topological superconductors. *Physical Review B*, 111(19):195419, 2025.